AD NUMBER

AD010749

NEW LIMITATION CHANGE

TO

Approved for public release, distribution unlimited

FROM

Distribution authorized to U.S. Gov't. agencies and their contractors; Administrative/Operational Use; APR 1953. Other requests shall be referred to Office of Naval Research, Arlington, VA 22203.

AUTHORITY

ONR ltr dtd 26 Oct 1977

AD-

10749

UNCLASSIFIED

CALIFORNIA INSTITUTE OF TECHNOLOGY

MECHANICAL ENGINEERING LABORATORY

OBSERVATIONS OF PROPAGATING STALL IN AXIAL-FLOW COMPRESSORS

by

T. Iura and W. D. Rannie

Report No. 4

April 1953

A REPORT ON RESEARCH CONDUCTED UNDER

CONTRACT WITH THE OFFICE OF NAVAL RESEARCH

OBSERVATIONS OF PROPAGATING STALL IN AXIAL-FLOW COMPRESSORS

Under Navy Contract N6 - ORI - 102 Task Order IV

Report No. 4

Prepared by:

Toru Iura

W. Duncan Rannie

Mechanical Engineering Laboratory
California Institute of Technology
Pasadena, California, April, 1953

ACKNOWLEDGEMENT

The authors wish to express their gratitude to Dr. Frank E. Marble and Professor Hsue-shen Tsien for many stimulating discussions concerning the propagating stall, and their thanks to Mr. F. T. Linton for his aid in the experiments and in preparing figures for the report.

SUMMARY

This report gives the results of experimental investigations of an axial-flow compressor in stall. Hot-wire anemometer measurements of the velocity fluctuations in stalled operation of an axial-flow compressor have demonstrated that stalling occurs for the most part in well-defined regions over the compressor annulus. These regions rotate without changing shape in the direction of the blade rotation with a speed proportional to, but of smaller magnitude than, the rotor speed. Two principle types of propagating stall were observed, one with the stalled region or regions extending over part of the blade height, the other with a single stalled region over the full blade height.

NOMENCLATURE

The following nomenclature is used in this report:

Symbol		Definition
A	=	compressor annulus area
C_a	=	axial velocity component
$\bar{C}_a$	=	axial velocity component averaged over the annulus
C_u	=	tangential velocity component
L	=	cycle length of velocity fluctuation
N_p	=	number of propagating stall regions
R	=	hot-wire resistance
R_a	=	wire resistance at air temperature
R_o	=	wire resistance at 0^o C
V	=	instantaneous velocity normal to radius of compressor
$\bar{V}$	=	mean velocity normal to radius of compressor
a, b	=	constants
c	=	airfoil chord length
i	=	heating current for hot-wire
p_s	=	static pressure
p_a	=	atmospheric pressure
r, R	=	radius of a particular stream tube
r_i, R_i	=	hub radius
r_o, R_o	=	tip radius
s	=	cascade pitch
u_o	=	velocity of rotor blade tip
Δ	=	change of a quantity
α	=	temperature coefficient of resistance of the wire material
ρ	=	fluid density
$\bar{\Phi}$	=	average flow coefficient = $\bar{C}_a / u_o$
ω	=	rotor angular velocity
ω_s	=	stalled region angular velocity
$\bar{\Psi}$	=	average power coefficient = $\dfrac{\text{Shaft Power}}{1/2\, \rho\, A\, \bar{C}_a\, u_o^2}$

TABLE OF CONTENTS

I. INTRODUCTION

Observations of stalling in axial-flow compressors have demonstrated that the regions of separated or reversed flow are not axially symmetric but occur in more or less well-defined patches around the circumference of the compressor annulus. The regions of retarded flow remain approximately the same shape and are propagated circumferentially with a velocity proportional to the rotor speed. This phenomenon, where the total flow rate through the annulus does not vary with time, will be called propagating stall. Surging will be defined as a phenomenon where the net flow through the entire annulus fluctuates with time. It is possible that surging involves an oscillation from one propagating stall pattern to another, the violence of the surge being determined by the natural frequency of the ducting or reservoirs in the compressor circuit. The propagating stall phenomena have been mentioned by other investigators although, to the authors' knowledge, the only paper reporting measurements is one given recently by Huppert and Benser (Ref. 1).

The investigations described here are concerned primarily with stall propagation; no distinct surge was observed. Probably more or less well-defined stall propagation phenomena occur in all axial-flow compressors as they are throttled beyond the peak pressure. Similar phenomena have been observed in centrifugal impellers and even in straight cascades by H. Emmons (private communication). Pressure or velocity measurements with instruments of low response time give no indication of the propagating stall. Hot-wire anemometers or high frequency pressure pick-ups are required for detection of the phenomena.

The propagating stall has been explained qualitatively as a successive unstalling and stalling of blades in a cascade. The stalled blade channels offer a high resistance to flow through the cascade and the approaching flow tends to be diverted to each side of the stalled region as shown in Fig. 1. The incidence angle is reduced to the left of the stalled blades and increased to the right. This tends to stall the next blade on the right and unstall the last stalled blade on the left. The stalled region hence moves to the right. Apparently, as the average flow angle of a

cascade approaches stalling incidence, the preferred flow pattern is one with groups of blades severely stalled alternating with groups of unstalled blades rather than a uniform stalling of all blades. The velocity of propagation of the stalled regions is determined by some characteristic time, the origin of which is not definitely understood at present. For a moving cascade, the stall propagation speed relative to a fixed system is the difference between the cascade speed and the propagation speed in the moving cascade. All propagating stall patterns observed moved relative to the compressor casing in the direction of the rotor with a speed less than the rotor speed (Fig. 2).

II. TEST EQUIPMENT

2:1 Test Compressor and Instrumentation

The compressor used in the stall propagation measurements was one designed to simulate internal flow patterns commonly employed in modern high performance turbomachines. A cross section of the test installation is shown in Fig. 3 where the principle dimensions are also summarized. The air flowed into the compressor through a cylindrical entrance duct with a bell mouth opening. A screen was installed on the bell mouth to prevent foreign objects from entering the compressor air stream. An interconnected set of four wall static pressure orifices was located midway through the entrance duct, which was calibrated to give the total air flow rate or flow coefficient. After acquiring an initial circumferential component from a set of pre-rotation vanes, the air flowed through successive rotating and fixed compressor blades as shown in Fig. 3. The exit portion of the installation consisted of a short cylindrical duct, an elbow section, and a transition section which connected the elbow to the throttle valve. The throttle valve which regulated the flow resistance and thus the compressor flow volume, consisted of two rectangular metal doors which could be actuated by a variable speed motor to vary the throttle opening and hence the flow rate.

A 125 H.P. electric dynamometer drove the compressor by means of a shaft which passed through the rear duct. The power input to the compressor could be found from accurate measurements of the rotative speed and of the driving torque which was determined by means of a diaphragm type force meter manufactured by the Hagan Corporation (see Ref. 2).

The compressor was constructed so that each blade was separately removable, hence a variety of blade and stage configurations were possible. Two types of blades were available, three stages of "free vortex" blading and one stage of "solid body" blading. Both sets were designed for an average power coefficient $\bar{\Psi} = 0.40$ at a flow coefficient $\bar{\Phi} = 0.45$. The design power coefficient was actually attained at $\bar{\Phi} = 0.43$ because of the influence of the wall boundary layers. The compressor blade tip diameter was 36 inches and the hub ratio 0.6. The blade solidity ranged from a

maximum of 1.150 at the rotor roots for both types to a minimum of 0.690 for the free vortex rotor tip and 0.903 for the solid body rotor tip. The blade sets are shown in Fig. 4, and the geometric properties are summarized in Table 1. There were 30 rotor blades and 32 stator blades in respective rows. The axial spacing between the center lines of adjacent blade rows was 2.875 inches. Most of the measurements were made at a compressor rotative speed of 750 rpm (u_o = 118 fps), hence compressibility effects were negligible, and the blades could be considered rigid as far as aerodynamic forces were concerned.

The entrance duct had a volume of 51 cu. ft. and the exit duct (between the compressor and the throttle), a volume of about 46 cu. ft. The calculated natural frequencies of the system considered as a Helmholtz resonator were above 22 cps except one mode involving coupling between the air volume and the drive shaft assembly, which was estimated as 18 cps. All propagating stall patterns, with one exception, had frequencies lower than the above. This one exception represented a metastable stall pattern which quickly reverted to one of lower frequency.

Instrument surveys downstream of each rotor and stator row were possible through the provision of six rectangular instrument ports located near the top of the outer case and a set of radial survey holes provided at several circumferential positions behind each blade row. A traversing carriage, described in Ref. 2, was used to position the instrument probe in the compressor ports; and a radial survey carriage, illustrated in Fig. 5, was used to position the probes in the radial survey holes.

The flow rate through the compressor was determined by measurements of velocity profiles which were correlated with the entrance duct wall static pressure. With a calibration chart of wall pressure vs. discharge rate, it was then possible to determine the flow rate by reading the wall pressure. The wall static pressure was measured with a water-micromanometer manufactured by the Meriam Instrument Company. This instrument, which is of the "movable well type", can be read to an accuracy of 0.001 inch of water.

Measurements of the exit-duct wall static pressure were made simultaneously with the torque measurements to obtain a quickly available idea of the pressure rise in the compressor. These pressures were measured with an electric pressure transducer manufactured by the

Statham Company, Los Angeles, California. The pressure detecting unit which consisted of a bridge circuit and a Brown "Electronik" precision indicator is shown at the right in Fig. 6 and described in detail in Ref. 3.

The foregoing information describes the salient features of the compressor installation as used for the stall propagation experiments. Further details may be obtained from Ref. 2 and 3.

2:2 Hot-Wire Equipment

For velocity fluctuation measurements, radial hot-wire anemometers utilizing platinum wires of 0.00024 in. diameter and 3/16 - in. length were employed. The hot-wire probe and its radial positioning carriage are shown in Fig. 5. The wires were manufactured by the Wollaston process, therefore were supplied with a silver jacket which was used to protect it during the manufacturer's drawing down process. Before using the wire, it was necessary to remove the outer jacket by immersing it in a nitric acid solution. The platinum wire was soft soldered to the supports and results indicated that it was sufficient to give a good mechanical and electrical bond.

A general view of the hot-wire instruments is shown in Fig. 6, and a schematic diagram of the apparatus is shown in Fig. 7. The hot-wire heating circuit and amplifier were designed and constructed by the Thiele-Wright-Rothbart Co. of Los Angeles, California. In the majority of the tests, a constant current of 50 milliamperes from a 90-volt B battery was used. The use of a relatively large battery source was to keep the current as nearly constant as possible, and this was found sufficient to limit current fluctuations to less than one percent even with large velocity changes.

The hot-wires were calibrated in the entrance duct of the compressor by finding values of its resistance under constant current conditions at several known values of air velocity. By plotting $R/R\text{-}R_a$ against $\sqrt{V}$, a straight line relationship was obtained, necessitating only a few points for the calibration (Fig. 8). This relationship is the conventional King's equation for the wire normal to the air stream:

$$i^2 \propto R_o \frac{R}{R - R_a} = a + b\sqrt{V}$$

The calibrations were made before and after each test run, and from the linear relationship obtained, a second curve of resistance (R) vs. air velocity (V) was plotted (Fig. 9), which was used to determine the velocity values under test conditions.

For phase measurements, two identical circuits were used so that simultaneous readings with two separate hot-wire probes could be made. The two circuits were checked for identity in response time so that phase measurements for the determination of the number of stalled regions could be made with two probes in different circumferential positions. This was done by feeding a common oscillator signal into both channels and checking the Lissajous figures created by the two output signals on an oscilloscope.

For the preliminary study of stall propagation, it was found convenient to use a direct-inking type oscillograph manufactured by the Brush Electronic Co., Cleveland, Ohio (Model BL-202). This, together with a Brush BL-905 amplifier had the advantage of making instantaneous, permanent chart records although the frequency response of the unit was flat only up to 100 cycles per second (see Fig. 10). This limited the response of the entire unit since the hot-wire amplifier had a flat frequency response up to about 1000 cycles per second as shown in Fig. 11. However, this response was felt adequate for the investigation of the observed pulsations ranging from 1.5 to 15 cycles per second.

The over-all calibration of the amplifier system was found by introducing known resistance changes (by means of a vibrating contactor) in the hot-wire line under actual operating conditions, and correlating this with the square wave signals produced on the oscillograph. The results of various calibrations for a given amplifier gain setting are shown in Fig. 12, where the peak input voltage to the oscillograph unit is plotted as a function of hot-wire resistance change. The oscillograph unit was provided with a calibration device which permitted any pen deflection to be translated in terms of input voltage. This, together with the hot-wire velocity response, provided the necessary information to interpret the oscillograph signals in terms of velocity fluctuations. Because of the low frequency response of the unit, it was not possible to record individual rotor wakes.

III. COMPRESSOR STALL WITH THREE-STAGE FREE VORTEX BLADING

3:1 Introduction

The experimental results obtained from the compressor with three stages of free-vortex blading will be discussed first, because this configuration produced the most clear cut examples of the various types of stall propagation observed. The regions of stall for this configuration are shown in Fig. 13a and b, which are plots of torque and exit-duct wall pressure as functions of flow coefficient at a compressor rotative speed of 750 rpm. It will be noted that the first signs of stall on closing the throttle occur in the form designated as "partial stall" at a flow coefficient slightly lower than the maximum torque and exit-duct pressure points. The region of partial stall extended to a flow coefficient slightly above $\bar{\Phi} = 0.30$, where the exit-duct wall pressure dropped off suddenly, and the compressor went into a regime designated as "full stall". The exit-duct wall pressure did not change appreciably in the full stall region. On closing the throttle, the compressor went into both partial and full stall at lower flow coefficients than when the flow rate was being increased at constant rotor speed. There was a definite hysteresis loop in the transitions between partial and full stalls. In terms of audible noise, partial stall was detectable by a rumbling noise that was slightly louder than the normal operating noise, and full stall was perceptible by a rumbling sound of very distinct periodicity.

3:2 Partial Stall

When the term "partial stall" is used, it is in the sense that only a part of the radial extent of the blade is experiencing stall. Hot-wire anemometer measurements showed periodic velocity fluctuations only in the region of the blades extending from the hub to about mid-radius. (Partial stall in the blade tip region was observed with other compressor blade configurations, as will be discussed later.) Initially, as the flow was throttled (at 750 rpm or 12.5 rps), the hub region disturbance had an average frequency of about 4.7 cycles per second. This disturbance extended to about mid-radius, and further throttling did not cause any appreciable change in the magnitudes of the velocity fluctuations. However,

the observed frequency increased to about 9.4 cycles per second, and on further throttling, became 14.1 cycles per second. Fig. 14 shows examples of the chart data obtained with the oscillograph. The principle types of partial stall patterns are shown as they appear with two different chart speeds of 25 mm per sec. and 125 mm per sec. The one-region partial stall fluctuations are shown at three different radii, and it can be seen that the fluctuations disappear entirely at mid-radius. The magnitudes of the instantaneous velocities, as measured, show strongly retarded flow regions that can result only from flow separation (stalling) on the blades. The mean velocity $\bar{V}$ is the average of the instantaneous velocities with respect to time over a complete cycle as determined by the mean resistance of the hot-wire. For velocity fluctuations large compared with the mean velocity, this procedure introduces some error. The portions of the velocity traces above the chart center line in general correspond to unretarded flow, while those below correspond to retarded flow. The amplitude of the velocity fluctuation ΔV was taken as the difference of the minimum velocities in the unretarded and retarded flow regions. The radial distribution of the velocity fluctuation amplitude ratios, $\Delta V/\bar{V}$, are shown in Fig. 15.

Two hot-wire anemometers were inserted to the same radii in a plane normal to the compressor axis as shown in Fig. 16 and their angular separation varied. The phase difference of the velocity patterns as measured with the two probes was equal to their angular separation for the fluctuations with frequency 4.7 cps, equal to twice the angular separation for the fluctuations with frequency 9.4 cps and three times the angular separation at 14.1 cps (see Fig. 17). The probe displaced in the direction of rotation lagged behind the other probe in all cases. It is clear from these observations that the three frequencies represent respectively one, two, and three propagating stall regions uniformly spaced around the circumference (Fig. 18).

Since the rotor speed was 12.5 rps in these tests, the partial stall regions rotated with 38 percent of the rotor speed in the direction of the rotor motion. Each of the three stalled patterns above was very stable in a narrow throttle range. The single pattern occurred in a very narrow flow coefficient range of about $0.40 > \bar{\Phi} > 0.39$ for closing throttle. The maximum width of the single region of retarded flow was about 17 percent

of the circumference, which corresponds to approximately 5 rotor blade channel widths. At a flow coefficient $\bar{\Phi} \cong 0.39$ the single stalled region became unstable and split into two regions which oscillated in their relative positions, but with further slight throttling, the two regions separated and finally took up stable positions 180 degrees apart. In this condition, the two regions were of nearly equal size and had the same maximum width, about 5 rotor blade channel widths. They did not differ significantly from the single region at the higher flow rate. The two-region partial stall was the stable pattern for the range of approximately $0.39 > \bar{\Phi} > 0.37$. At $\bar{\Phi} \cong 0.37$ the two-region pattern became unstable, a further splitting and rearrangement occurred, and on very slight throttling, a three-region pattern of retarded flow became the stable pattern. The maximum width of each of the three regions, which were 120 degrees apart, corresponded to about 4 rotor blade channel widths (Fig. 18). The radial extent of each of the regions increased slightly with closing throttle, however, the maximum velocity fluctuation ratio at the hub was about the same ($\Delta V/\bar{V} \cong 0.65$) for all three types (Fig. 15). On closing the throttle to a flow coefficient $\bar{\Phi} \cong 0.30$ the three-region pattern became unstable and full stall (described later) appeared.

When the throttle was opened from the full stall point, the above patterns appeared in reverse order, although the limits of ranges of succeeding patterns occurred at larger flow rates than on closing throttle. The three-region pattern appeared at $\bar{\Phi} \cong 0.34$ and the one-region pattern disappeared at $\bar{\Phi} \cong 0.41$. In one instance, four symmetrical propagating stall regions appeared on opening the throttle from the full stall. Although well-defined, the pattern was soon replaced by the three-region pattern without touching the throttle (see Fig. 14).

The blades tended to stall near the hub first as the throttle was closed. Apparently an alternating pattern of stall is more stable than an axially symmetric stall. The strong retardation of the flow in the stalled region causes an increased flow rate and hence an unstalling tendency over the remainder of the annulus. It might be thought that further throttling would simply increase the size of the stalled region. However, the circumferential pressure distribution behind the stalled blade row must be controlled largely by the unstalled axially symmetric flow beyond the mid-radius, and this, one would expect to be nearly uniform around the circumference. Unrestricted growth of the single partial stalled

region would lead to a strong asymmetry incompatible with the symmetry of the flow beyond mid-radius. Hence, the increased area of the region of stall appeared as two equal regions symmetrically placed as if in an effort to keep the pressure as uniform as possible. Further throttling caused three symmetrically placed patterns to appear for similar reasons. Evidently, a completely axially symmetric stall is unstable compared with the alternating stalled regions and the minimum width for a single stalled region corresponds to 4 or 5 rotor blade channels. As long as the outer portion of the annulus is unstalled, the area of the single stalled region cannot grow indefinitely, but multiple patterns of the minimum area stalled region can arise, tending to keep the over-all flow and in particular the pressure as symmetrical as possible. The stalled regions were very sharply defined and demonstrated characteristics of certain types of non-linear oscillations. A given throttle setting allowed two alternative patterns and very slight disturbances caused one or the other to appear. Closing or opening the throttle a small amount eliminated one or the other completely.

3:3 Full Stall

As the compressor was throttled, a sharp transition occurred at a flow coefficient of $\bar{\Phi} \cong 0.30$ from partial stall to full stall. Full stall is characterized by a propagating stall region that extends over the entire blade height. The average exit-duct pressure showed no significant change from this point to complete shut-off while the torque continued to decrease slightly and then increased uniformly to shut-off. The propagating speed of the full stall did not change significantly, ranging from 26 percent of the rotor speed at the initiation of full stall to 30 percent of the rotor speed at shut-off. At any given flow coefficient in the full stall region, the propagating speed was the same whether the flow rate was reached by opening the throttle or closing the throttle (see Fig. 19).

The extent of the region of retarded flow in full stall at a flow coefficient $\bar{\Phi} = 0.323$ (opening throttle) is shown in Fig. 20 and 21. The region is widest at the hub where it occupies about 12 rotor blade channel widths and its width decreases toward the tip where it occupies 2 rotor blade channel widths. The growth of the retarded flow region at mid-blade height as the flow coefficient is decreased is traced in Fig. 22.

The width of the stall region increases from about 7 rotor blade channel widths at the beginning of full stall to almost 26 channel widths at shut-off. Fig. 23 shows sample oscillograph records of velocity fluctuations in the full stall regime. It will be noted that the retarded flow region is characterized by irregular velocity fluctuations.

The magnitudes of the velocity fluctuations in full stall were nearly constant over the entire blade length ($\Delta V/\bar{V} \cong 0.7$) as contrasted with the situation in partial stall, where the velocity fluctuations decreased in magnitude radially from the hub (Fig. 15). The velocity fluctuations in full stall at mid-blade height behind the first and the third rotors are compared in Fig. 24. The magnitude of the peak velocity fluctuation amplitude ratio, $\Delta V/\bar{V}$, was larger behind the third rotor than behind the first rotor indicating a more severe disturbance in the rear stages. Undoubtedly reverse flow occurred in the full stall regime, particularly at low flow rates. The hot-wire records do not show this clearly since velocity magnitudes alone were measured. Visual observations of cotton tufts inserted in the compressor air stream showed the presence of reversed flow at low over-all flow rates, mostly toward the hub.

An investigation of the influence of the volume of ducting was made in early tests. Blocking off the rear of the compressor annulus increased the full stall propagating velocity from 30 percent of the rotor speed to about 40 percent. Blocking off both front and rear of the compressor annulus so as to eliminate all effects of ducting resulted in a propagation velocity of about 45 percent of the rotor speed. Although these drastic restrictions have some influence, it is evident that the propagating stall is primarily a characteristic of the blading and its occurrence is independent of the presence of ducts.

If surging occurred, the frequency would be expected to be high, that is 20 or 30 cps, corresponding to the resonator frequencies of the ducting and much higher than the frequencies of passage of the propagating stall at the rotor speeds used. No surging was recognized in any of the flow regimes above, although there is a possibility that surging occurred in some of the configurations discussed later.

3:4 Effect of Removing the Third Stator Row

Upon removing the blades of the third stator row, that is the last row of the three-stage free vortex blading, the most significant effect was that no multiple partial stall patterns occurred. A single rather unstable partial stall appeared at the hub at a flow coefficient $\bar{\Phi} \cong 0.38$ on closing the throttle. This flow coefficient was smaller than that marking the beginning of partial stall with the third stator in place. Full stall commenced at $\bar{\Phi} \cong 0.36$, a higher flow coefficient than with the third stator. The propagation velocity of both partial and full stall regimes were nearly equal and both slightly greater than the full stall velocity with the third stator (Fig. 19). Similar to the case with the third stator in place, partial stall occurred at a flow coefficient slightly lower than the maximum exit-duct pressure point, however, the exit-duct pressure decreased at a faster rate with closing throttle until the full stall point, where it dropped off suddenly. The exit-duct wall pressure also showed a hysteresis effect at the transition points between partial and full stalls.

3:5 Effect of Solidity

By removing alternate blades from each blade row in the three-stage free vortex compressor, it was possible to observe the effect of a change in solidity on the stall propagation. Partial stall of the multiple type was not found although a region of small irregular velocity fluctuations was observed on throttling at a flow coefficient $\bar{\Phi} \cong 0.35$. The variation of propagating stall speed with flow coefficient is shown in Fig. 25. Full stall commenced at $\bar{\Phi} \cong 0.33$ with one stalled region propagating in the direction of compressor rotation at 27 percent of the rotor speed. The propagation speed decreased with throttling until $\bar{\Phi} \cong 0.29$, from which point it remained constant at slightly under 20 percent of the rotor speed. At $\bar{\Phi} \cong 0.07$, the one-region propagating full stall deteriorated into a rather irregular type of disturbance. Fig. 26 shows a comparison of the propagating stall speed at $\bar{\Phi} \cong 0.20$ (midway in the stall regime) with that for a full complement of blades. The stall speed in terms of the measured velocity fluctuation frequency is shown as a function of the rotor speed. The linear relationship between the propagating stall speed and the compressor rotor speed is evident here, and it is

seen that decreasing the solidity by one-half decreased the propagation speed from 28 percent to 20 percent of the rotor speed.

Fig. 27 shows how the stall region width at mid-radius increased from 3 rotor blade channel widths at the start of stall to about 8 blade channels at the lower limit of propagating stall. Below this flow rate, the entire annulus evidently was in stall and it was impossible to detect any regularity in the velocity fluctuations. Fig. 28 illustrates the radial variation of the stall region width at a flow coefficient $\bar{\Phi} = 0.253$. The width is a maximum at the hub and is equivalent to the width of about 7 rotor blade channels, and a minimum at the outer radius where it is equivalent to about 3 rotor blade channel widths. Under these conditions, the width at mid-blade height is approximately equal to 4 blade channels.

The effect of removing the third stator row is shown in Fig. 25, where the propagating stall speed shows an increase throughout the propagating stall region except at the upper flow limit. At $\bar{\Phi} = 0.20$, this increase is from slightly under 20 percent to slightly above 22 percent of the rotor speed. This increase was similar to that observed with the full solidity. Removal of the third stator row also appeared to have the effect of maintaining a more constant stall speed throughout the propagating stall region. With full solidity for stator blades, one-half solidity for rotor blades and the third stator row in place, the propagating stall speed was 23 percent of the rotor speed (at $\bar{\Phi} \cong 0.20$).

IV. COMPRESSOR STALL WITH ONE STAGE OF BLADING

4:1 One-Stage Free Vortex Blading

The regions of stall for the compressor with one stage of free vortex blading alone are shown in Fig. 29, which is a plot of the exit-duct wall pressure as a function of the flow coefficient. Stall initially occurred with closing throttle at the peak pressure point in the form of a single propagating stall region at the outside of the annulus rather than at the hub. This pattern commenced at $\bar{\Phi} \cong 0.31$ with a propagating stall speed of about 48 percent of the rotor speed as shown in Fig. 30. The single pattern had a maximum retarded flow region width of about 2 rotor blade channels and extended from the outer radius to about mid-blade height. Further throttling to $\bar{\Phi} = 0.303$ resulted in the formation of two stalled regions propagating at about the same speed as the single region, and placed 180 degrees apart in their most stable position. At $\bar{\Phi} = 0.298$, a single-region stall pattern again appeared with a lower propagation speed equal to about 36 percent of the rotor speed. From Fig. 30, it will be noted that the propagation speed for both types of partial stall decreases somewhat with closing throttle. The results of phase measurements made to determine the number of stalled regions for the foregoing cases are plotted in Fig. 31. It should be noted that although the phase difference measured for a single stall cycle may be in considerable error due to instability of the flow, the average value of a number of a points for any position of the hot-wire probes gave very reasonable results. Each point in Fig. 31 represents the average value of five or more phase angle measurements.

Examples of the oscillograph records for the partial stall phenomena are given in Fig. 32. Fig. 33 is a plot of the velocity fluctuation amplitude ratio as a function of radius for the three afore-mentioned partial stall cases. For all the partial stall patterns, the velocity fluctuation amplitude ratio $\Delta V/\bar{V}$ was greatest at the tip ($\Delta V/\bar{V} \cong 0.6$), although for the lower flow one-region pattern a second maximum point of $\Delta V/\bar{V} \cong 0.6$ appeared at $R/R_o = 0.9$ or 1.8 inches from the tip. The first two partial stall patterns extended only to about mid-radius as evidenced from the velocity fluctuations, however, the one-region pattern occurring at

$\bar{\Phi}$ = 0.298 showed a gradual decrease in velocity fluctuations towards the hub and did not diminish until a point very close to the hub. At the lower limit of this regime ($\bar{\Phi} \cong 0.26$), two-region stall patterns appeared, but they were rather unstable.

On further throttling to the flow coefficient range $0.26 > \bar{\Phi} > 0.11$, irregular velocity fluctuations were observed primarily in the outer part of the annulus. Although this constituted stalling of the partial type, it was difficult to tell whether any propagation similar to the previous cases was involved. An example of the radial distribution of the velocity fluctuations for this regime is shown in Fig. 34 for the flow coefficient $\bar{\Phi} \cong 0.12$. The velocity fluctuations in this regime covered a greater portion of the compressor annulus than the previous cases, although it still decreased to a negligible value at the hub. The top chart in Fig. 35 is an example of the irregular velocity fluctuations found in this regime.

Full stall did not occur until $\bar{\Phi} \cong 0.11$ where a single region of retarded but fluctuating flow disturbance extending over the entire blade height appeared with the very low propagation speed of about 10 percent of the rotor speed. Examples of the velocity fluctuations found in this full stall regime are shown in the oscillograph records of Fig. 35. The retarded flow region does not appear to be caused by a single well-defined stall disturbance, but rather by a series of irregular stalled regions grouped together. The velocity fluctuations were very irregular in this retarded flow region, although investigations with an apparatus of higher frequency response might ascertain whether or not these fluctuations were a result of disturbances from all of the blades. The width of the fluctuating retarded flow region increased towards the outer radius, and in Fig. 36 this radial variation is plotted for a flow coefficient $\bar{\Phi}$ = 0.112. At this flow rate, the region of retarded flow had a width of about 6 rotor blade channels at the hub and increased to cover the entire annulus at the tip. The peak velocity fluctuation amplitude ratio did not vary radially to a great extent (see Fig. 34), having a maximum value of about 0.6 at mid-blade height.

Closing the throttle further (from $\bar{\Phi}$ = 0.112) increased the width of the region of retarded flow at the hub from 6 rotor blade channel widths to about 22 channel widths at $\bar{\Phi}$ = 0.075 (see Fig. 37). Below this flow rate, irregular flow seemed to occur over the entire annulus.

In terms of audible noise, a definite periodic beat could be heard when the compressor was in full stall, but only a continuous rumbling sound was noticeable below this regime.

When the throttle was opened from shut-off, the sequence of stall phenomena appeared in reverse order but at slightly higher flow rates (see Fig. 29). The exit-duct wall pressure values were slightly lower going out of full stall than when the throttle was being closed, however, this was the only point at which the exit-duct wall pressure showed any hysteresis effect.

4:2 One-Stage Solid Body Blading

With one stage of solid body blading, the stall occurred first in the outer part of the annulus as the compressor was throttled. Fig. 38, which plots exit-duct wall pressure as a function of flow coefficient, shows that propagating stall initially occurs at about the point of maximum exit-duct pressure at a flow coefficient $\bar{\Phi} \cong 0.31$. The top chart in Fig. 39 is an example of the type of velocity fluctuation existing at the initial stall point. The stall patterns at the tip ($R/R_O = 0.98$) were rather unstable so that consistent determinations of frequency were impossible. However, the initial stall appearing at $\bar{\Phi} \cong 0.31$ tended to be one with a propagating speed of about 45 percent of the rotor speed. Upon closing the throttle to the flow coefficient $\bar{\Phi} \cong 0.30$, no very stable pattern appeared although there was some evidence of a pattern with two regions of retarded flow. Further throttling beyond the flow coefficient $\bar{\Phi} \cong 0.27$, gave only irregular fluctuations of the flow velocities concentrated, for the most part, in the outer portion of the annulus. This behavior was quite similar to that observed with one stage of free vortex blading. The exit-duct wall static pressure decreased gradually from its maximum value with closing throttle until $\bar{\Phi} \cong 0.13$ where full stall first appeared. There were no distinct variations in the exit-duct wall pressure in the partial stall region as was observed with one stage of free-vortex blading, just as there were no distinct types of partial stall patterns.

In Fig. 40, the radial variation of the velocity fluctuation amplitude ratio, $\Delta V/\bar{V}$, is shown for the initial unstable one-region partial stall at $\bar{\Phi} \cong 0.31$ and also for the unstable two-region partial stall occurring

at $\bar{\Phi} \cong 0.30$. The velocity fluctuations are a maximum at the tip and decrease rapidly from $R/R_o = 0.9$ towards the hub. Similar to the partial stall cases for the other blade configurations, the maximum value of $\Delta V/\bar{V}$ was about 0.6. The velocity fluctuation ratio for the irregular partial stall regime ($0.27 > \bar{\Phi} > 0.13$) had about the same variation as that for one-stage free vortex blading, however, the maximum value of $\Delta V/\bar{V}$ remained constant over a larger portion of the annulus. This is illustrated for the flow coefficient $\bar{\Phi} \cong 0.16$ in Fig. 41.

Full stall occurred at $\bar{\Phi} \cong 0.13$ upon closing the throttle with one region of retarded fluctuating flow propagating in the direction of compressor rotation with a speed of about 12 percent of the rotor speed. The velocity fluctuations for full stall were similar to those observed with one stage of free vortex blading, as shown on the bottom row of chart records in Fig. 39. The velocity fluctuation amplitude ratio remained fairly constant over the compressor radius and had a maximum value, $\Delta V/\bar{V} \cong 0.65$ (see Fig. 41). The propagating stall speed decreased with closing throttle to about 9 percent of rotor speed at the lower flow limit of full stall, as shown in Fig. 42.

As for the single-stage free vortex blading, the width of the retarded flow region near the hub increased on closing the throttle from 9 rotor blade channel widths to extend over the entire annulus at $\bar{\Phi} \cong 0.050$ (see Fig. 43). In Fig. 44, the radial variations of the retarded flow region width are shown for two cases, one for the highest flow rate in full stall and the other near the lower flow rate limit. In both cases, the retarded flow region was a minimum at the hub and increased to cover the entire circumference at about $R/R_o = 0.9$, then decreased again to cover approximately 20 rotor blade channel widths at the tip.

Closing the throttle below $\bar{\Phi} \cong 0.050$ brought irregular flow throughout the annulus which made determinations of definite flow patterns impossible. The exit-duct wall pressure increased slightly at this point as shown in Fig. 38. Similar to the case for the free vortex blading, on opening the throttle, the reverse sequence of stall phenomena occurred at slightly higher flow coefficients than when the throttle was being closed. The exit-duct wall pressure had a lower value going out of full stall than when the flow was being throttled, and this was the only hysteresis effect observed in the exit-duct pressure characteristic.

V. SUMMARY OF THE EXPERIMENTAL RESULTS

Propagating stall occurred in the form of more or less well-defined regions of retarded flow which rotated without changing shape in the direction of blade rotation with a speed proportional to, but of smaller magnitude than, the rotor speed. Two principle types of stall were observed which are defined as "Partial Stall" and "Full Stall".

Partial Stall characteristics are:

1. Partial stall occurs at higher flow coefficients than full stall.
2. The stalled region or regions extend over only a part of the blade height.
3. One or more stalled regions may exist.
4. The stalled region may be concentrated either at the root or the tip, depending on the blade and compressor configuration.
5. The propagating stall speed is higher than that for the full stall type.
6. Transition into partial stall upon closing the throttle occurs at or slightly beyond the maximum exit-duct pressure and is accompanied by a small or gradual decrease in pressure.
7. The size of the stalled region or regions increases with decrease in flow coefficient until a transition point is reached where one of the following happens:
   a. The region or regions regroup into the next larger number of regions propagating at about the same speed.
   b. The multiple-region pattern regroups into one partial stall region propagating with a lower speed (this was found for one-stage free-vortex blading).
   c. The partial stall regions regroup into a single region of the full stall type.
8. The maximum velocity fluctuation amplitude ratio, $\Delta V/\bar{V}$, was about the same for all cases ($\Delta V/\bar{V}$ = 0.6 to 0.65).

Full Stall characteristics are:

1. The stalled region extends over the full blade height.
2. Only one stalled region exists.
3. The propagating stall speed is lower than that for partial stall.

4. Transition into full stall is accompanied by a drop in exit-duct pressure upon closing the throttle, and a hysteresis loop is found when exit-duct pressure variations for opening and closing throttle are compared.
5. The propagating stall speed does not change appreciably with flow coefficient.
6. The propagating stall speed is reduced with a decrease in solidity (three-stage free vortex blading).
7. The size of the retarded flow region increases with decrease in flow coefficient.
8. At any given flow coefficient in the full stall regime, the retarded flow region is widest at the radial position where partial stall is widest.
9. The maximum value of the velocity fluctuation amplitude ratio, $\Delta V/\bar{V}$, is about 0.7.

All stall phenomena observed were not of the well-defined propagating stall type. Results from one stage tests indicated a partial stall which was not well-defined, and at very low flow coefficients a poorly-defined full stall. It is not certain whether the irregular velocity fluctuations observed in these instances result from the propagating stall, a high frequency surge, or a combination.

VI. DISCUSSION OF THE EXPERIMENTS

The extreme complexity of the various propagating stall patterns makes detailed explanation impossible at the present time. Sears (Ref. 6) and Marble (Ref. 7) recently have made theoretical studies of propagating disturbances in two-dimensional cascades. Sears assumed an infinite number of blades, and although Marble treated the case of a finite number, this refinement amounts to only a small correction. Both investigations were based on perfect fluid flow but with different assumptions concerning the behavior of the unsteady lift with angle of attack. Sears introduced a phase lag between the fluctuating lift and the mean angle of attack and determined the propagating speed in terms of this phase lag which was left undetermined. Marble introduced a non-linear dependence of lift on angle of attack and on rate of change of angle of attack so a hysteresis loop was formed. The propagating speed was found in terms of an arbitrary characteristic time in the lift relation.

In both of the above theories, the characteristic time was undetermined. It was believed that this was connected with the time required for establishment of a separated boundary layer when an airfoil of the cascade was subjected to a sudden change of angle of attack. In the past, experiments have been run with single airfoils oscillating through angles of attack so the airfoils alternately stalled and unstalled. The phase lag between lift and angle of attack in these experiments is of the right order of magnitude to explain the propagating stall but precise correspondence is not very close. Further, some of the results from the compressor experiments seem inconsistent with a characteristic time of this type. In particular, removal of every second blade in the compressor should result in doubling the stall propagating speed if the above were correct, and no such result was observed. The comparative constancy of the full stall propagating speed with flow rate over such a wide range requires a characteristic time that is quite insensitive to large changes of mean angle of incidence and even to reversed flow, and this seems rather inconsistent with the time required for establishment of a boundary layer.

Apparently the characteristic time is relatively independent of the number of blades and of the detailed nature of the flow through the blades. Hence a characteristic time connected with the inertia (or

apparent mass) of the flow approaching the cascade has been suggested as more reasonable. The shifting of the stream lines far in front of the cascade by alternate blocking and unblocking of the flow through the cascade should not be strongly dependent on the cascade solidity or on the detailed nature of the flow in the cascade itself. Marble is currently investigating a model of this type. Actually, more definite experimental evidence is required to show that the inertia effect does determine the characteristic time. The presence of more than one blade row may influence the experimental findings and it is planned to make a study of one rotor blade row alone in the next series of tests.

For the solidities ordinarily occurring in axial-flow compressors the two-dimensional cascade turning angles are fairly well represented by assuming the leaving angle is independent of the incidence angle, even in stalled operation. This representation is simpler to use than the lift coefficient corrected for cascade interference. The loss in total pressure through a compressor cascade is small and approximately constant over a range of incidence angle of 8° to 10°, but rises sharply outside this range. The observations of propagating stall are typical of non-linear oscillations. Since the most marked non-linear characteristic of the flow is found in the total pressure loss variation, it seems probable that this characteristic is important in determining the amplitudes of the stall fluctuations.

Knowledge of the leaving angle and of the total pressure loss as functions of incidence angle do not help to determine the characteristic time controlling the propagating speed but this representation of the cascade flow seems to have advantages over the earlier approaches of Sears and Marble. At the suggestion of the senior author, Sears made an analysis (Ref. 8) based on constant leaving angle for the flow rather than lift coefficient. He did not introduce the total pressure loss, however, so neither the amplitude of the fluctuations nor the propagating speed were determined.

All the propagating disturbances observed, of course, involved both rotor and stator blade rows, but the propagation speeds were such that it is not certain whether the rotor or the stator was primarily responsible. There was some tendency for the width of the regions of retarded flow to be integral multiples of the rotor blade channel widths

at the hub and blade tip in full stall, and hence it is believed that the disturbances were propagating on the rotor. The stator blades had a very marked influence in determining whether or not a given stall pattern occurred, as demonstrated by the striking results of removal of the third stator blade row. This prevented the multiple partial stall patterns at the hub from occurring, even five blade rows ahead.

Although the full stall flow regime was the most stable as far as range of flow was concerned, at least with more than one stage installed, the partial stalls are in many ways more interesting. The partial stall occurs at the larger flow rates and would occur more frequently in normal compressor operation than the full stall. Further, it is generally agreed that blade failures are more likely to occur at flow rates corresponding to the beginning of stall and, hence, probably in the partial stall regimes. In the past, many believed that blade failure was caused primarily by a stalled flutter with only one mode of vibration excited by the self-induced aerodynamic forces. From the observations of the partial stall, it is clear that large aerodynamic excitation can arise without self-induced flutter of individual blades. It seems quite possible that the partial stall may be responsible for blade failure rather than the stalled flutter. What effect blade flexibility would have on partial stall is not known. The various partial stall patterns observed were of a metastable type and a blade natural frequency in the range of partial stall frequencies might influence the relative stability of the partial stall regimes very greatly. It is clear that to reduce aerodynamic excitation of rotor blades, it is preferable to have the partial stall occur at the hub rather than the blade tip. The free vortex rotor blades have constant chord from root to tip although this is not the general practice. In the multistage tests, the partial stall occurred at the hub whereas with the more conventional tapering blades, it might well occur at the tip. The relatively high solidity of the free vortex blading and even higher solidity of the solid body blading toward the tip were not sufficient to prevent tip stall in the single-stage configurations.

The effective wave-lengths of the partial stall and even more of the full stall patterns are so large that the influence of the propagating stall cannot be confined to a single blade row, because the distance

between center lines of the blade rows is a small fraction of the pattern wave length. Hence, stall on a single blade row can influence rows far ahead as well as far behind. It is difficult at this moment to predict how the knowledge of the propagating stall will influence future compressor design. It may be possible to suppress some of the stall patterns, but it is not even known if this would improve or worsen over-all performance. More experiments on a variety of compressors are required to determine which of the various stall phenomena are characteristics of all compressors and which are characteristics of particular machines.

It would be expected that a different characteristic line of static pressure rise versus flow rate would be found for each distinct type of stall pattern. Since the transition from one stall pattern to another occurs at different flow rates, depending on whether the flow is decreasing or increasing, hysteresis loops should be found at the flow rates corresponding to the transitions. The most distinct loop found in the experiments corresponded to the transition between partial and full stall in the three-stage free vortex configuration. Smaller hysteresis loops were found in the one-stage configurations and although none could be detected in the transitions of multiple patterns in the partial stall range, it would be surprising if they did not exist even if small. Since surging depends on the existence of a hysteresis loop, it seems possible that surging involves an oscillation between two different stall patterns. The surging frequency is usually, if not always, the natural frequency of some resonator connected with the compressor. The conditions for occurrence of self-induced oscillations and their amplitudes, resulting from the presence of hysteresis loops, are not known.

VII. REFERENCES

1. "Some Stall and Surge Phenomena in Axial-Flow Compressors", by M. C. Huppert and W. A. Benser, NACA, preprint of paper presented at the 21st Annual Meeting of the Institute of Aeronautical Sciences, New York City, January, 1953.

2. "Theoretical and Experimental Investigations of Axial Flow Compressors", by J. T. Bowen, R. H. Sabersky, and W. D. Rannie, Report on Research Conducted under Contract with the Office of Naval Research, California Institute of Technology, January, 1949.

3. "Theoretical and Experimental Investigations of Axial Flow Compressors, Part 3, Progress Report on Loss Measurements in Vortex Blading", by C. C. Alsworth and T. Iura, Report on Research Conducted under Contract with the Office of Naval Research, California Institute of Technology, July, 1951.

4. "Investigations of Axial-Flow Compressors", by J. T. Bowen, R. H. Sabersky, and W. D. Rannie, Transactions of the ASME, Vol. 73, No. 1, January, 1951, pp. 1-15.

5. "Review of Hot-Wire Anemometry", by J. B. Willis, Australian Council for Aeronautics Report ACA-19, October, 1945.

6. "On Asymmetric Flow in an Axial-Flow Compressor Stage", by W. R. Sears, ASME Preprint, Paper No. 52-F-15, presented at ASME Fall Meeting, September, 1952.

7. "Propagation of Stall in Compressor Blade Rows", by F. E. Marble, California Institute of Technology, paper presented at Institute of Aeronautical Sciences' 21st Annual Meeting, New York City, January, 1953.

8. "A Theory of 'Rotating Stall' in Axial-Flow Compressors", by W. R. Sears, Report under Contract AF 33 (038)-21406, Graduate School of Aeronautical Engineering, Cornell University, 1953.

FREE VORTEX $\left[C_{u1} = .145 \frac{r_0}{r} u_0 ;\ C_{u2} = .345 \frac{r_0}{r} u_0\right]$

	ROTOR					STATOR				
SECTION LOCATION - r - INCHES	10.8	12.6	14.4	16.2	18.0	10.8	12.6	14.4	16.2	18.0
DESIGN ENT. ANGLE - ROTOR - β_1 - DEG.	51° 21′	42° 24′	36° 2′	31° 21′	27° 45′					
DESIGN ENT. ANGLE - STATOR - γ_2 - DEG.						38° 3′	42° 24′	46° 13′	49° 34′	52° 31′
DESIGN EXIT ANGLE - ROTOR - β_2 - DEG.	86° 49′	65° 17′	50° 40′	41° 3′	34° 29′					
DESIGN EXIT ANGLE - STATOR - γ_1 - DEG.						61° 46′	65° 17′	68° 4′	70° 18′	72° 8′
SECTION CAMBER - θ - DEGREES	46° 40′	31° 0′	20° 19′	13° 47′	9° 48′	31° 53′	31° 6′	29° 59′	28° 41′	27° 20′
CASCADE STAGGER ANGLE - β' - DEG.	74° 48′	57° 54′	46° 12′	38° 15′	32° 36′					
CASCADE STAGGER ANGLE - γ - DEG.						54° 0′	57° 57′	61° 12′	63° 55′	66° 11′
SOLIDITY - C/S	1.150	.985	.862	.766	.690	1.035	.970	.920	.880	.849
MAXIMUM THICKNESS - % C	12	11	10	9	8	10	10	10	10	10

SOLID BODY $\left[C_{u1} = .325 \frac{r}{r_0} u_0 ;\ C_{u2} = \left(.325 \frac{r}{r_0} + .200 \frac{r_0}{r}\right) u_0\right]$

	ROTOR					STATOR				
SECTION LOCATION - r - INCHES	10.8	12.6	14.4	16.2	18.0	10.8	12.6	14.4	16.2	18.0
DESIGN ENT. ANGLE - ROTOR - β_1 - DEG.	52° 10′	46° 18′	40° 30′	34° 42′	28° 43′					
DESIGN ENT. ANGLE - STATOR - γ_2 - DEG.						48° 22′	46° 15′	42° 40′	37° 21′	29° 18′
DESIGN EXIT ANGLE - ROTOR - β_2 - DEG.	83° 7′	70° 47′	58° 19′	45° 33′	31° 48′					
DESIGN EXIT ANGLE - STATOR - γ_1 - DEG.						69° 30′	65° 18′	60° 36′	55° 11′	48° 41′
SECTION CAMBER - θ - DEGREES	40° 52′	32° 45′	24° 6′	14° 49′	4° 15′	28° 23′	25° 53′	24° 37′	24° 42′	27° 0′
CASCADE STAGGER ANGLE - β' - DEG.	72° 36′	62° 41′	52° 33′	42° 7′	30° 51′					
CASCADE STAGGER ANGLE - γ - DEG.						62° 34′	59° 12′	54° 59′	49° 42′	42° 48′
SOLIDITY - C/S	1.150	1.061	.995	.944	.903	1.039	.970	.920	.880	.850
MAXIMUM THICKNESS - % C	12	11	10	9	8	10	10	10	10	10

Table 1 Geometric Properties of the Blade Sets

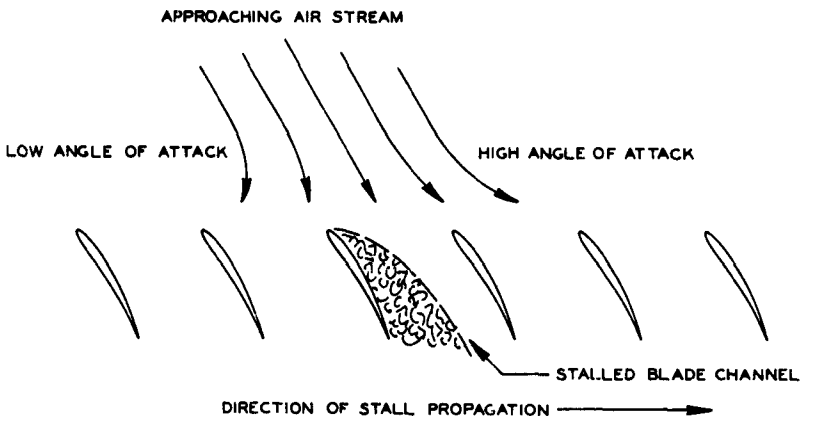

Fig. 1: Stall Propagation in a Cascade

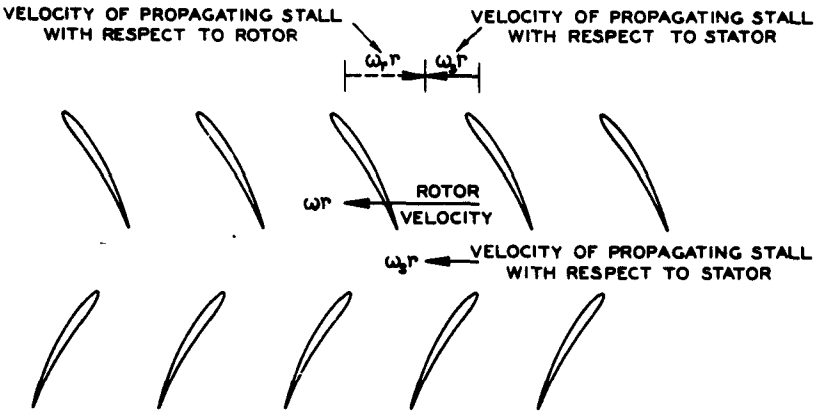

Fig. 2: Stall Propagation in Compressor Blade Rows

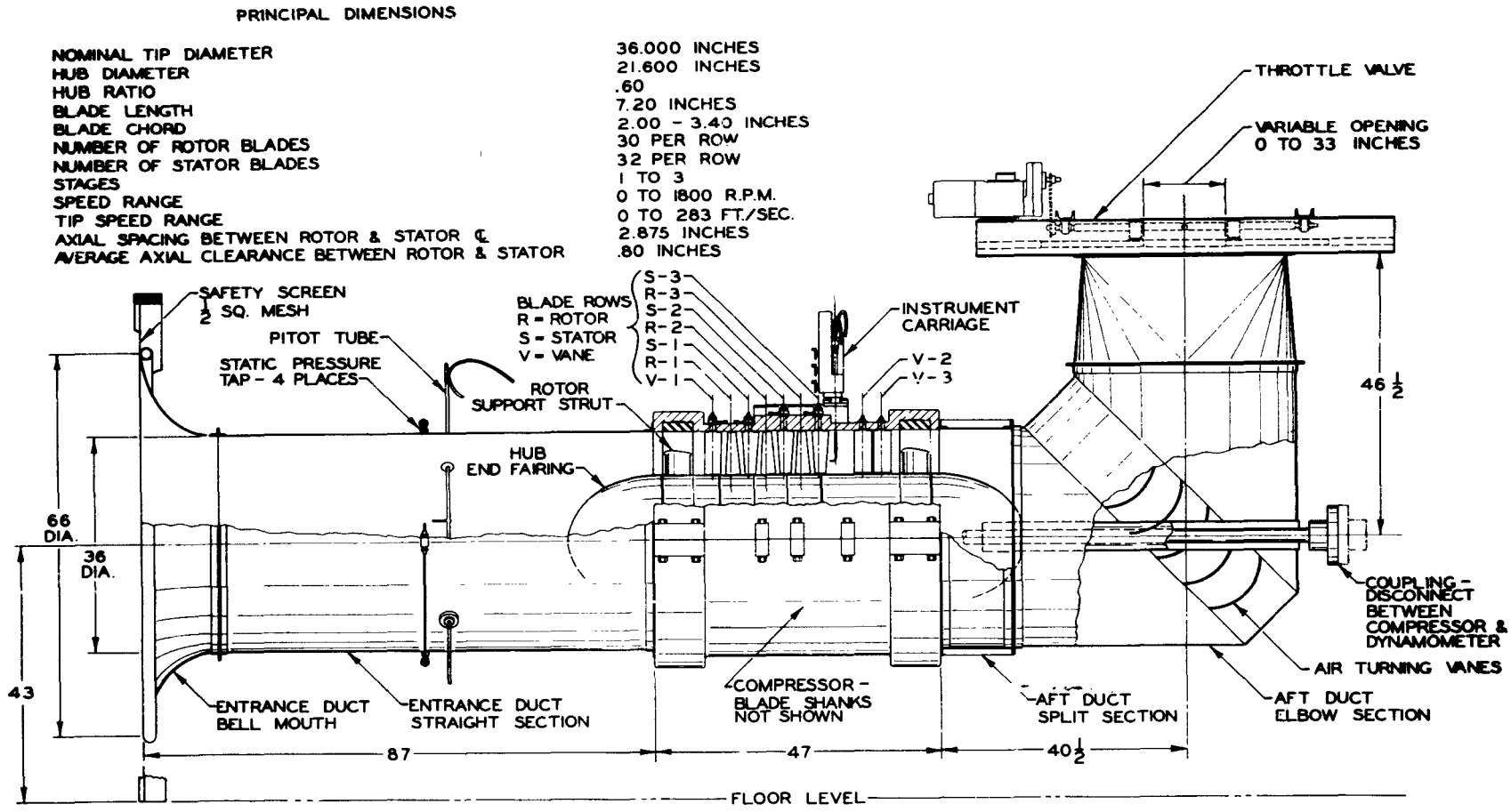

Fig. 3: Assembly Drawing of the Test Installation

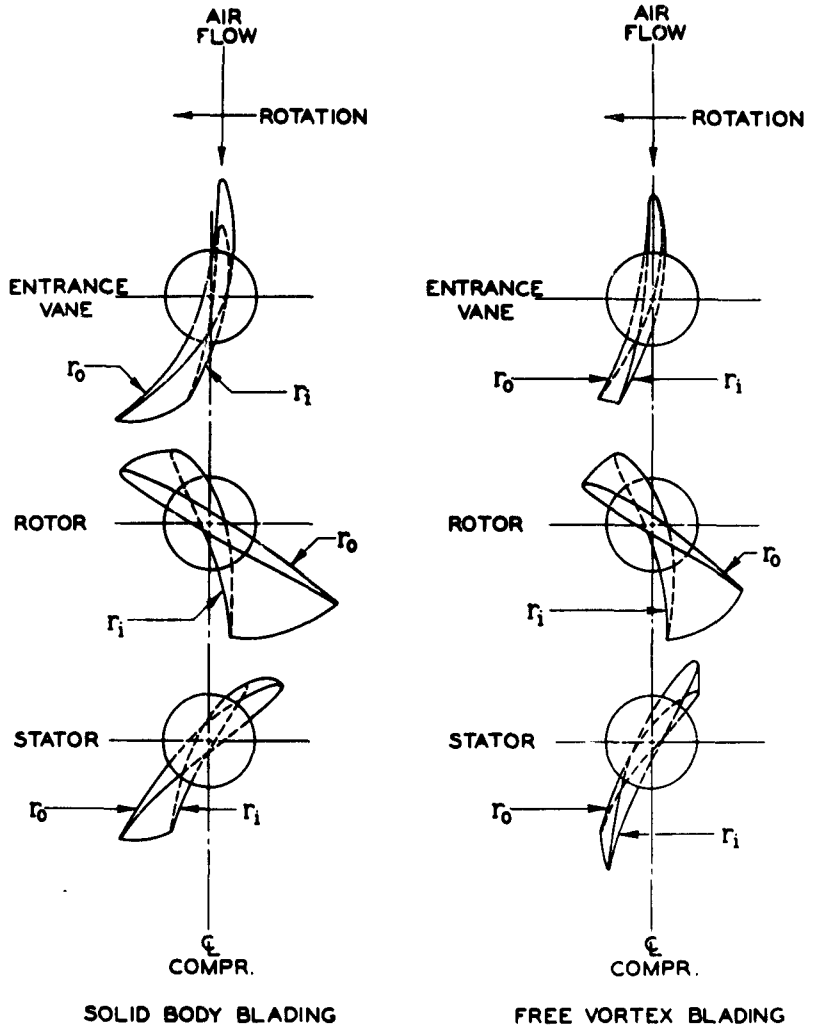

Fig. 4: Root and Tip Sections of the Two Types of Compressor Blading

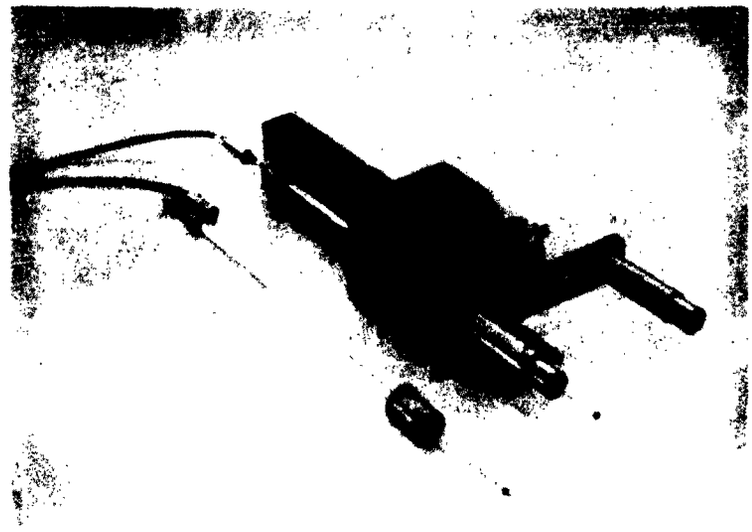

Fig. 5: Hot Wire Anemometer Probes and Radial Survey Carriage

Fig. 6: General View of Instruments: (A) Pressure Detecting Unit, (B) Hot-Wire Heating Circuit and Amplifier, (C) Potentiometer, (D) Oscillograph

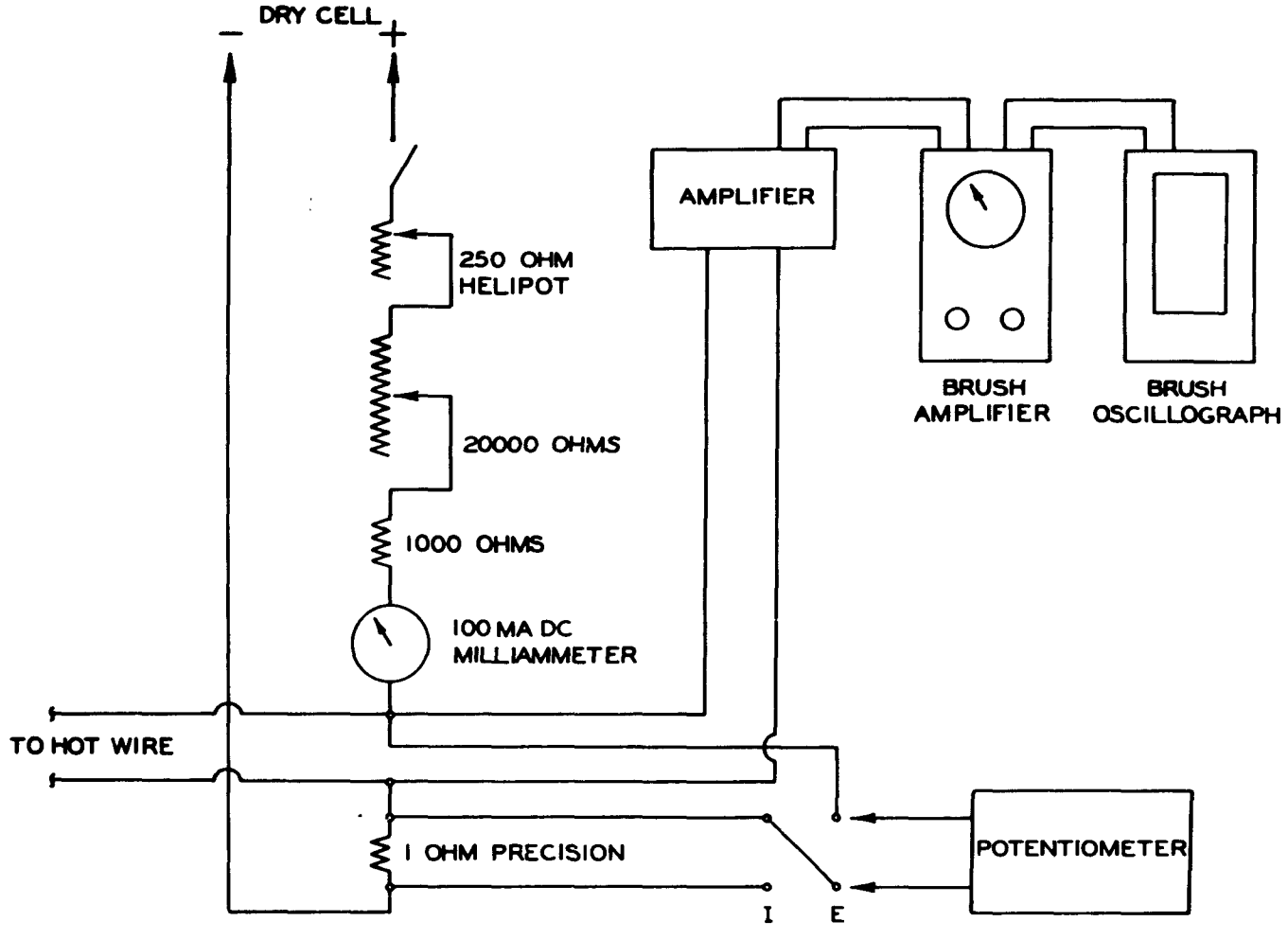

Fig. 7: Schematic Diagram of Hot Wire Apparatus

FIGURE 8
CALIBRATION CURVE OF 0.00024 INCH PLATINUM WIRE
FOR CONSTANT CURRENT OPERATION
PLOTTED FOR CONFORMITY WITH KING'S EQUATION

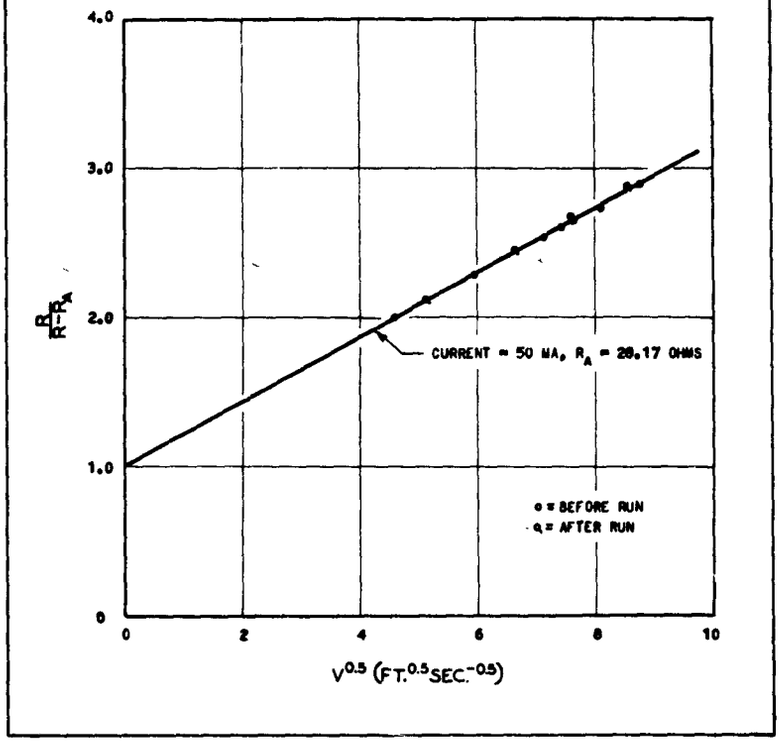

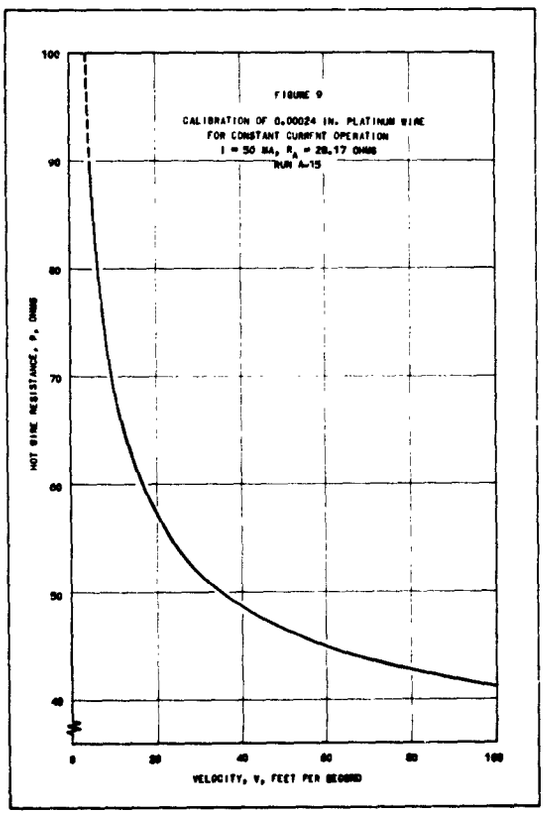

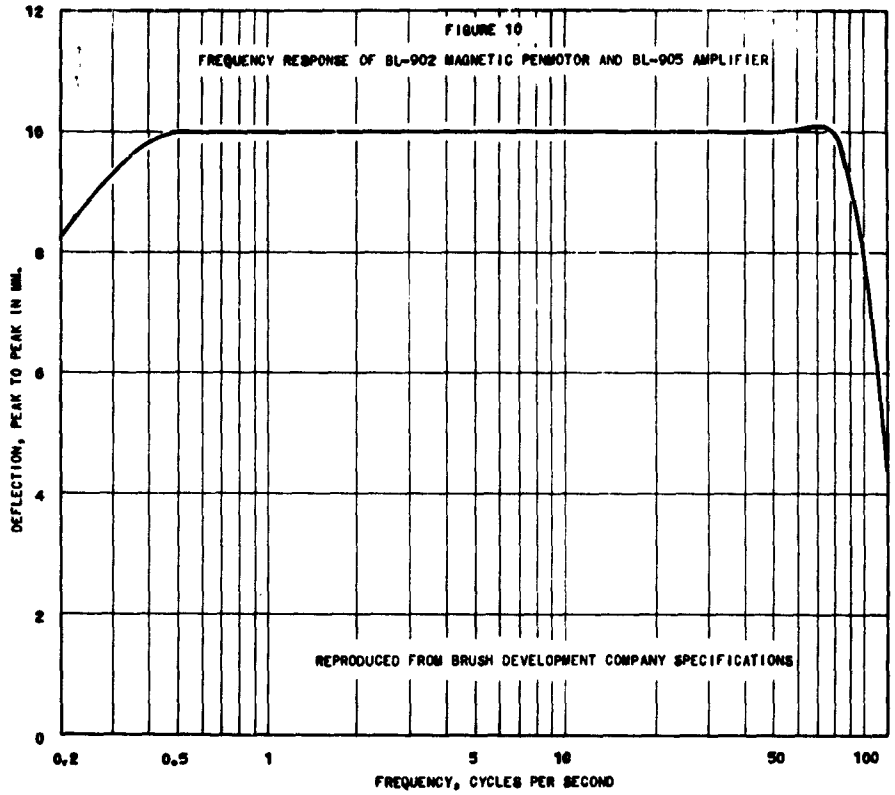
FIGURE 10
FREQUENCY RESPONSE OF BL-902 MAGNETIC PENMOTOR AND BL-905 AMPLIFIER
DEFLECTION, PEAK TO PEAK IN MM.
12
10
8
6
4
2
0
0.2
0.5
1
5
10
50
100
FREQUENCY, CYCLES PER SECOND
REPRODUCED FROM BRUSH DEVELOPMENT COMPANY SPECIFICATIONS

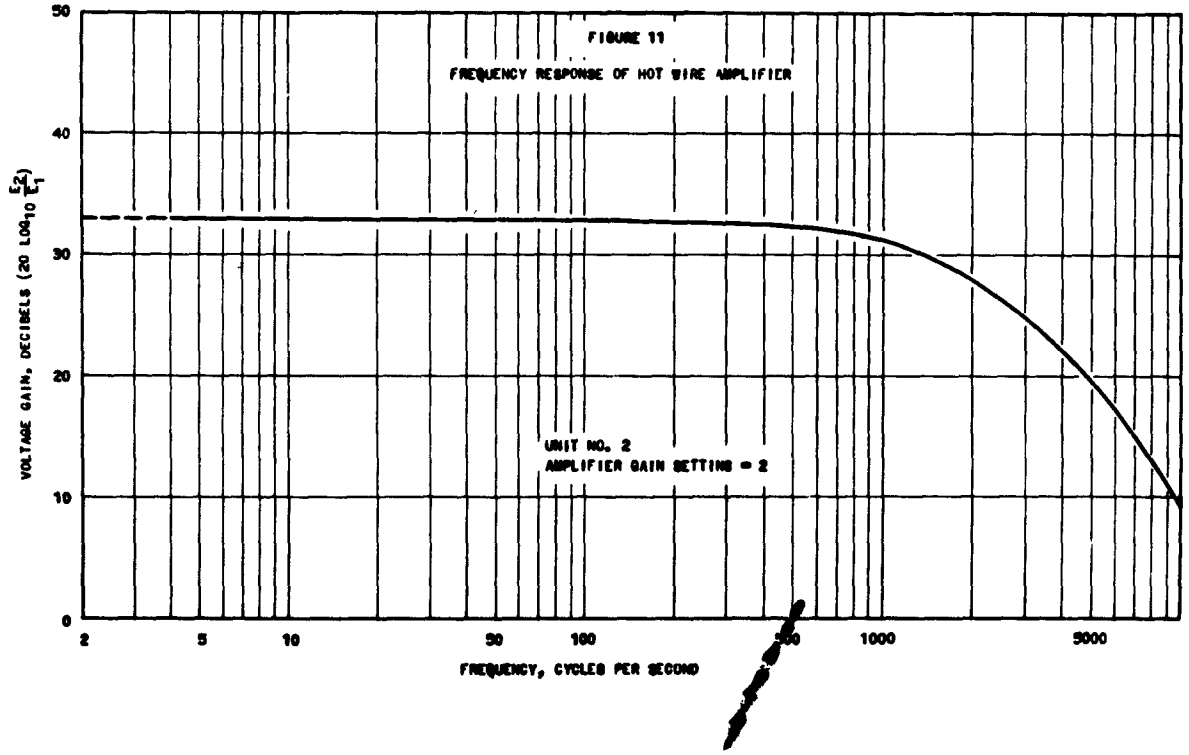
FIGURE 11
FREQUENCY RESPONSE OF HOT WIRE AMPLIFIER
VOLTAGE GAIN, DECIBELS (20 LOG10 E2/E1)
50
40
30
20
10
0
2
5
10
50
100
500
1000
5000
FREQUENCY, CYCLES PER SECOND
UNIT NO. 2
AMPLIFIER GAIN SETTING = 2

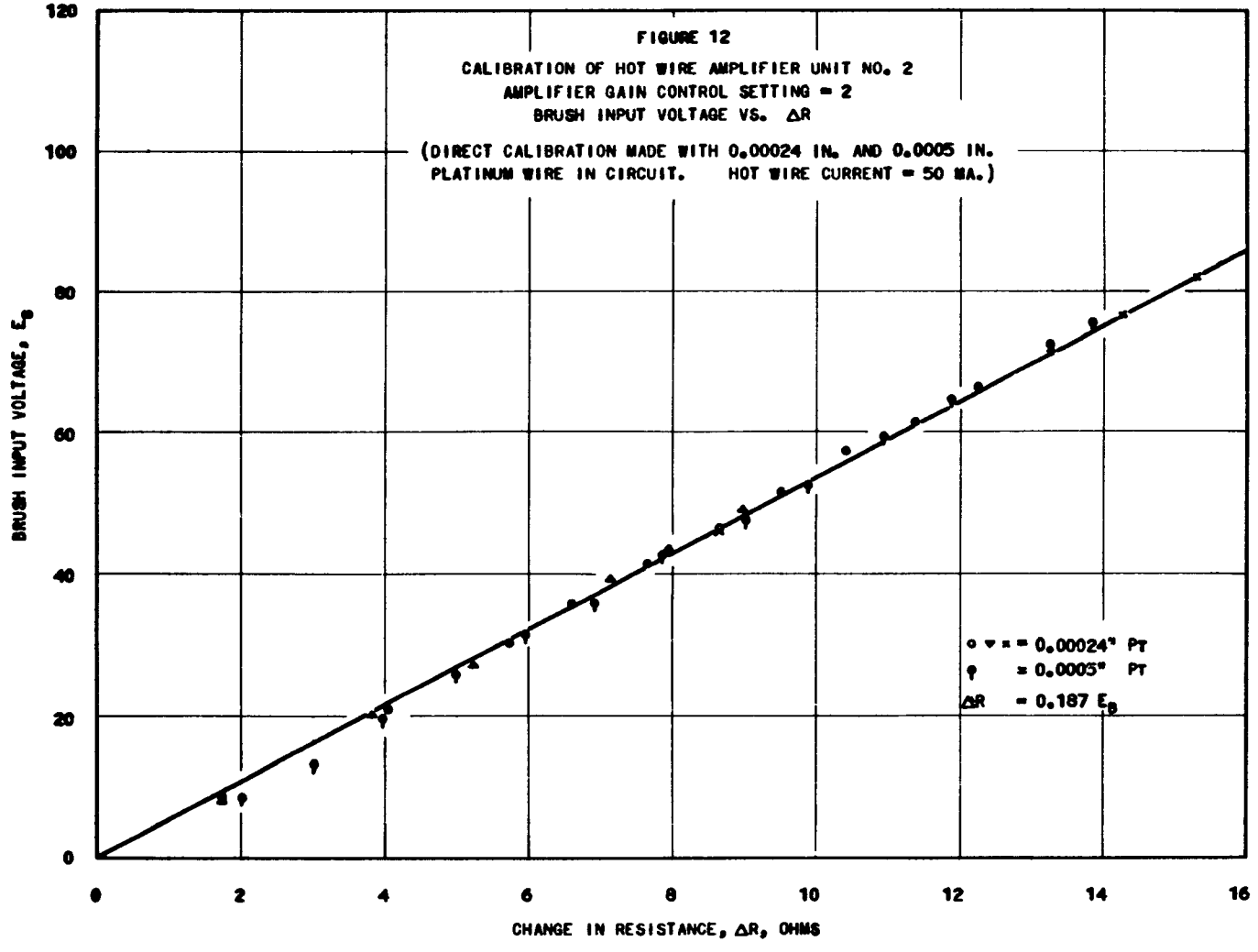
FIGURE 12
CALIBRATION OF HOT WIRE AMPLIFIER UNIT NO. 2
AMPLIFIER GAIN CONTROL SETTING = 2
BRUSH INPUT VOLTAGE VS. ΔR
(DIRECT CALIBRATION MADE WITH 0.00024 IN. AND 0.0005 IN.
PLATINUM WIRE IN CIRCUIT. HOT WIRE CURRENT = 50 MA.)
BRUSH INPUT VOLTAGE, E_B
CHANGE IN RESISTANCE, ΔR, OHMS
0
20
40
60
80
100
120
0
2
4
6
8
10
12
14
16
o ▾ x = 0.00024" PT
φ = 0.0005" PT
ΔR = 0.187 E_B

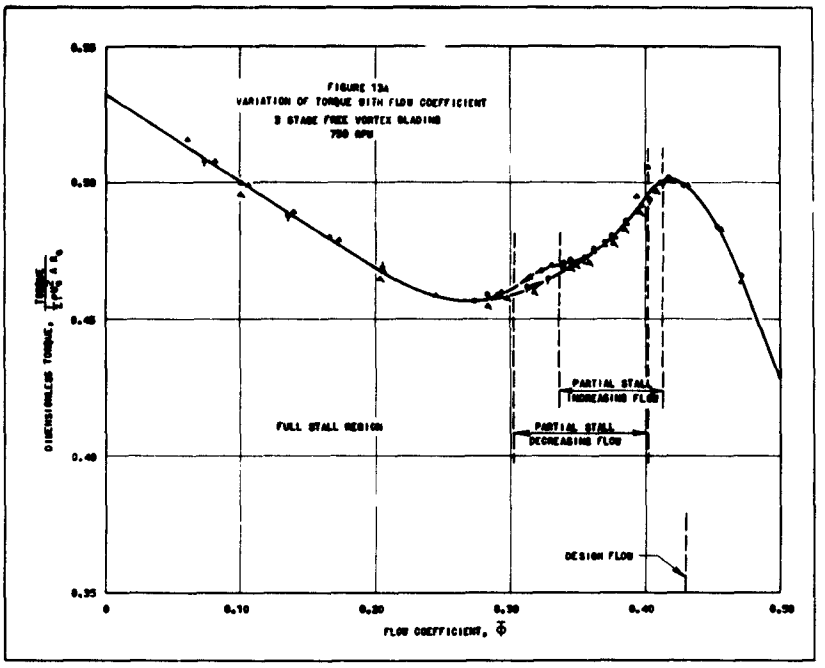
FIGURE 13a
VARIATION OF TORQUE WITH FLOW COEFFICIENT
3 STAGE FREE VORTEX BLADING
700 RPM
DIMENSIONLESS TORQUE, $\frac{\text{TORQUE}}{\frac{1}{2}\rho U_m^2 A R_m}$
FULL STALL REGION
PARTIAL STALL INCREASING FLOW
PARTIAL STALL DECREASING FLOW
DESIGN FLOW
0.35
0.40
0.45
0.50
0
0.10
0.20
0.30
0.40
0.50
FLOW COEFFICIENT, $\bar{\Phi}$

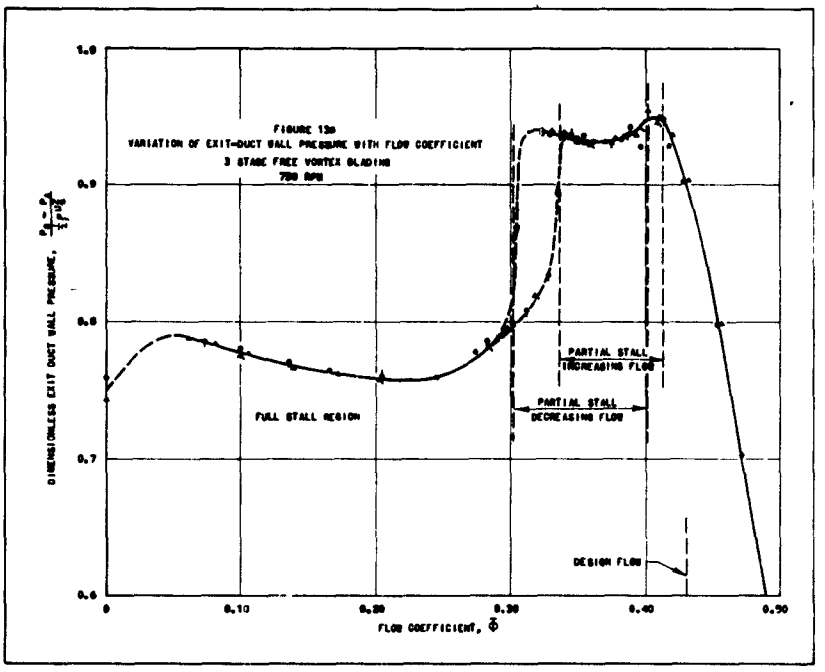
FIGURE 13b
VARIATION OF EXIT-DUCT WALL PRESSURE WITH FLOW COEFFICIENT
3 STAGE FREE VORTEX BLADING
700 RPM
DIMENSIONLESS EXIT DUCT WALL PRESSURE, $\frac{P_2 - P_1}{\frac{1}{2}\rho U_m^2}$
FULL STALL REGION
PARTIAL STALL INCREASING FLOW
PARTIAL STALL DECREASING FLOW
DESIGN FLOW
0.6
0.7
0.8
0.9
1.0
0
0.10
0.20
0.30
0.40
0.50
FLOW COEFFICIENT, $\bar{\Phi}$

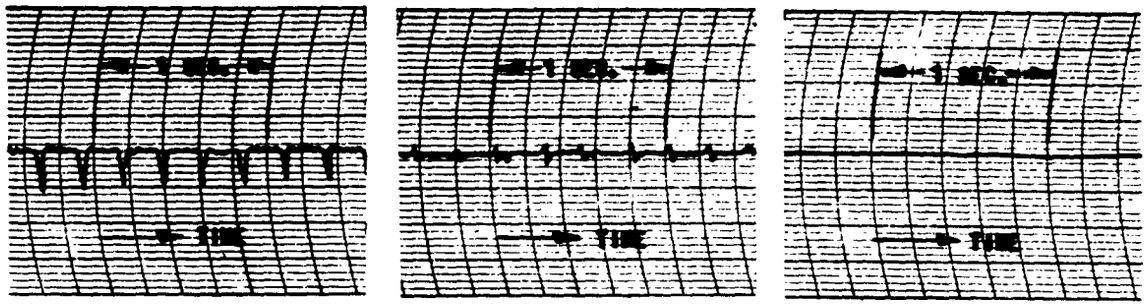

$R/R_0 = 0.65$ $R/R_0 = 0.75$ $R/R_0 = 0.80$

ONE-REGION PARTIAL STALL, $\bar{\Phi} = 0.397$, INITIAL STALL POINT AT CLOSING THROTTLE, PROPAGATING STALL SPEED = 38 PERCENT OF ROTOR SPEED

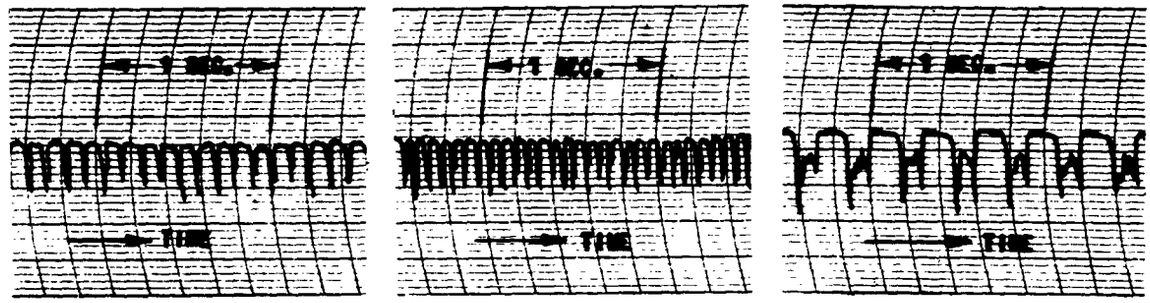

TWO-REGION PARTIAL STALL
$\bar{\Phi} = 0.38$, $R/R_0 = 0.65$
$\omega_s = 0.38\,\omega$

THREE-REGION PARTIAL STALL
$\bar{\Phi} = 0.36$, $R/R_0 = 0.65$
$\omega_s = 0.38\,\omega$

FULL STALL
$\bar{\Phi} = 0.29$, $R/R_0 = 0.65$
$\omega_s = 0.26\,\omega$

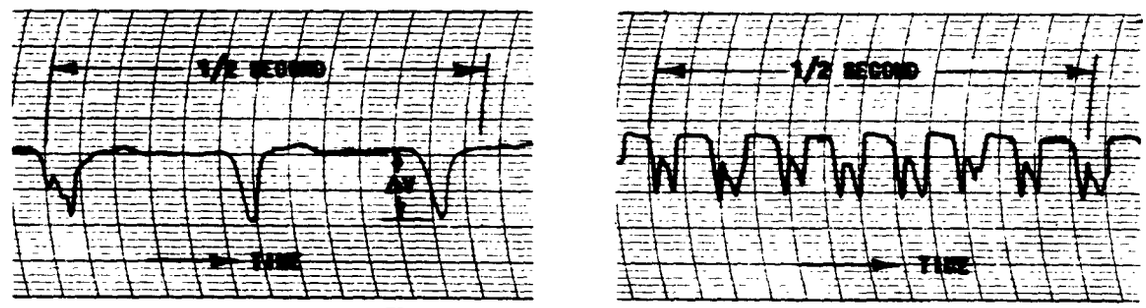

ONE-REGION PARTIAL STALL, $\bar{\Phi} = 0.39$
$R/R_0 = 0.65$, $\omega_s = 0.38\omega$, FAST CHART SPEED

THREE-REGION PARTIAL STALL, $\bar{\Phi} = 0.34$
$R/R_0 = 0.65$, $\omega_s = 0.36\omega$, FAST CHART SPEED

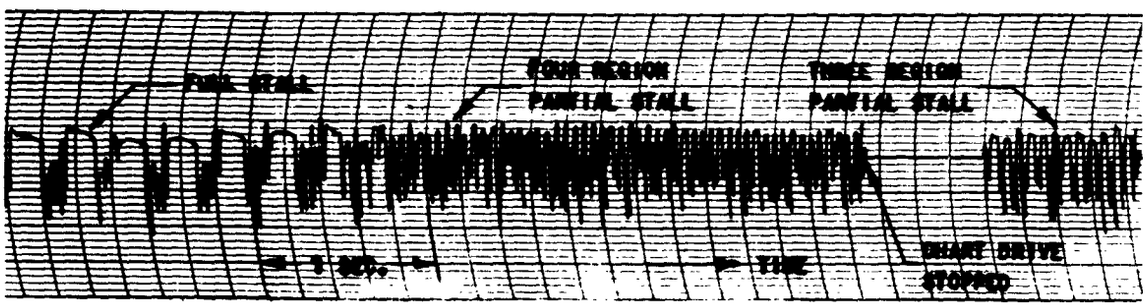

EXAMPLE OF UNSTABLE STALL PATTERN AT TRANSITION POINT. THROTTLE SETTING UNTOUCHED. CHANGE FROM FULL STALL TO THREE-REGION PARTIAL STALL WITH INTERMEDIATE FOUR-REGION PARTIAL STALL PATTERN. OPENING THROTTLE, $\bar{\Phi} = 0.339$, $R/R_0 = 0.611$, CONSTANT RPM.

FIGURE 14: OSCILLOGRAPH RECORDS OF PROPAGATING STALL. THREE-STAGE FREE VORTEX BLADING, BEHIND THIRD ROTOR ROW, 750 RPM

FIGURE 15
RADIAL VARIATION OF PEAK VELOCITY FLUCTUATION AMPLITUDE RATIOS
THREE-STAGE FREE VORTEX BLADING, 750 RPM
BEHIND THIRD ROTOR ROW

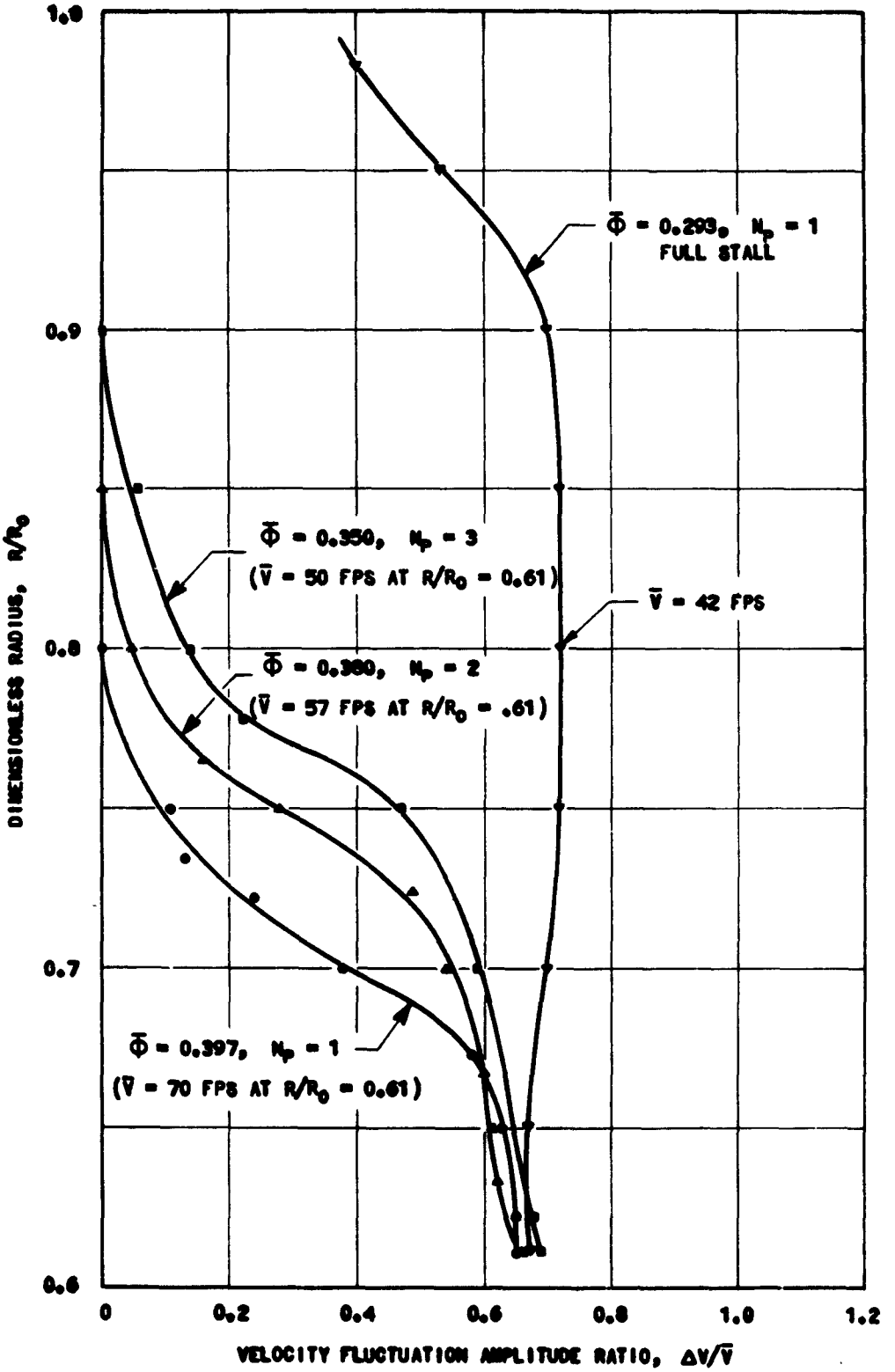

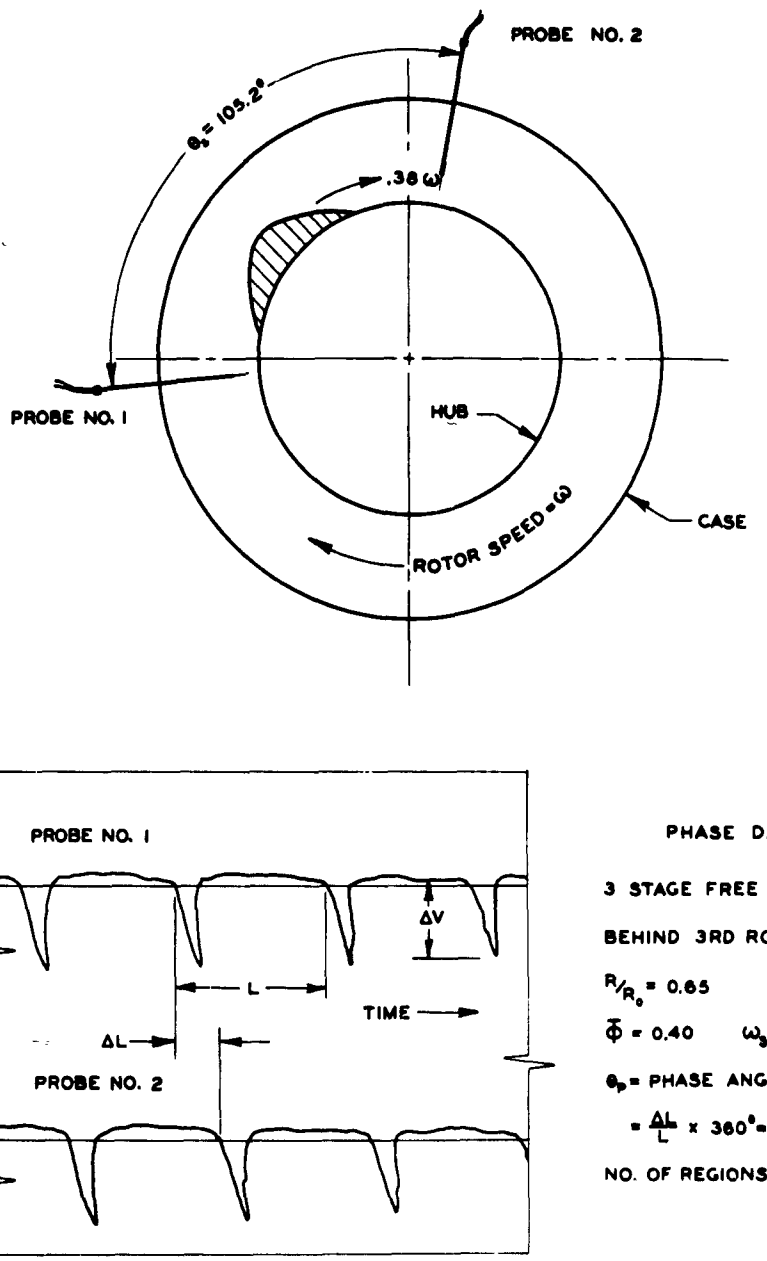

Fig. 16: Illustration of Phase Measurements for the Determination of the Number of Stalled Regions

FIGURE 17

RESULTS OF PHASE MEASUREMENTS FOR THE DETERMINATION OF STALL DISTURBANCE NUMBER

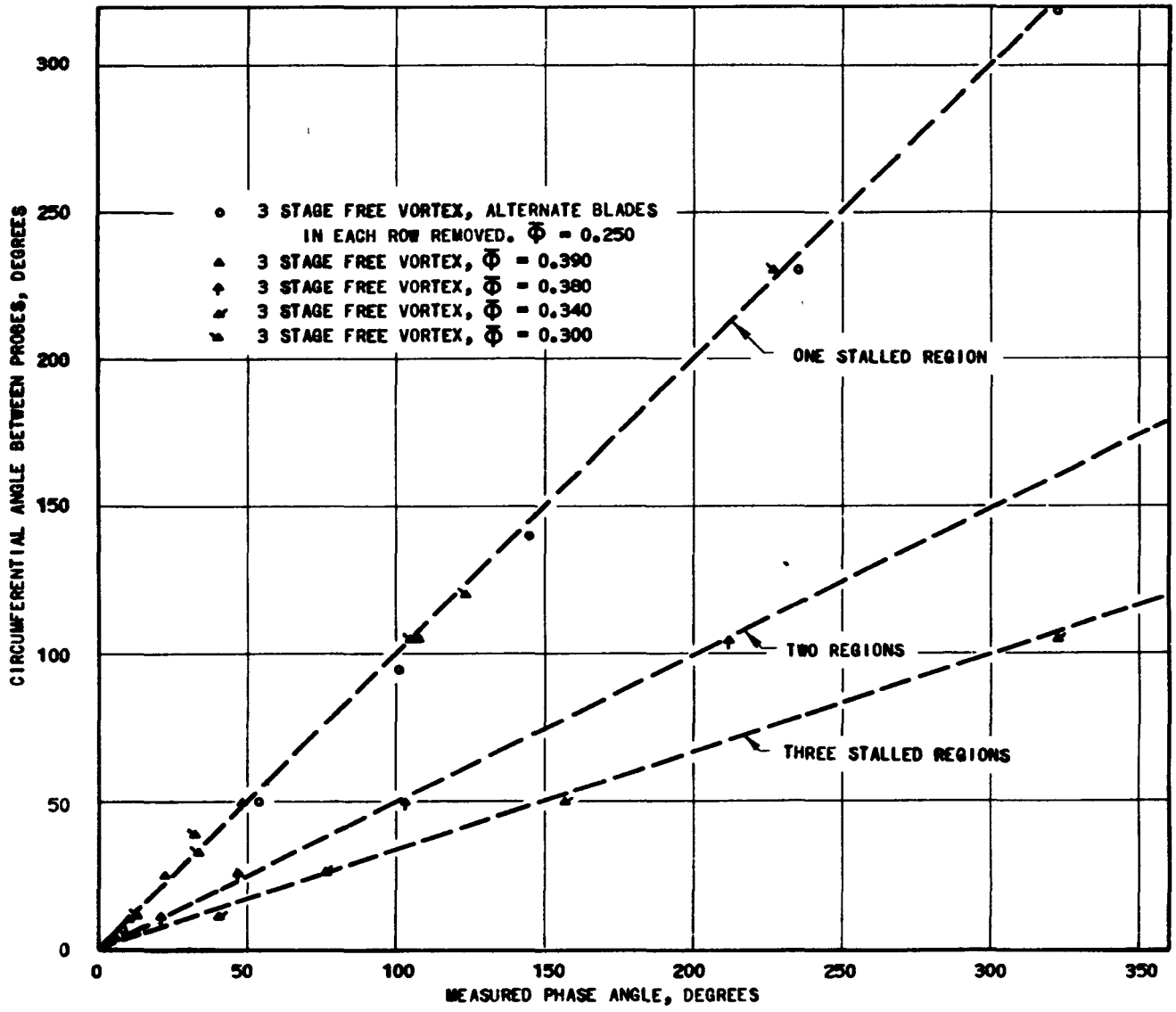

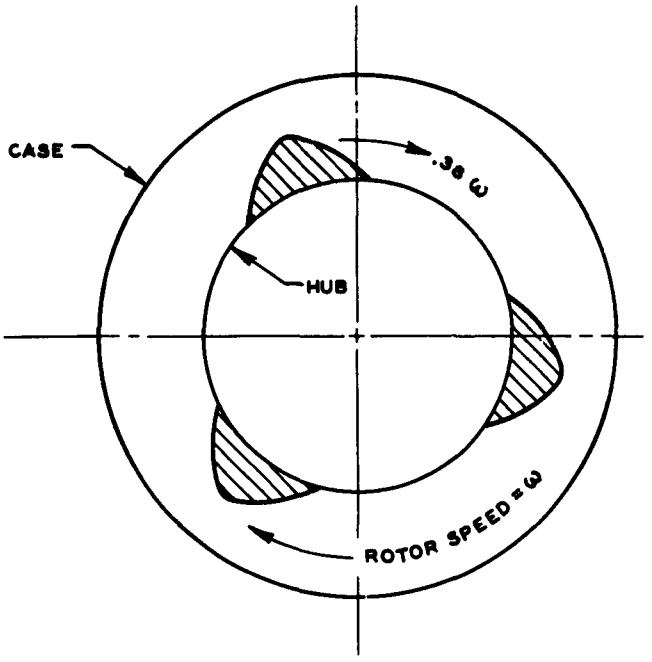

Fig. 18: Depiction of Three-Region Propagating Stall Pattern. Three-Stage Free Vortex Blading, $\bar{\Phi} = 0.363$ Behind Third Rotor Row, 750 rpm.

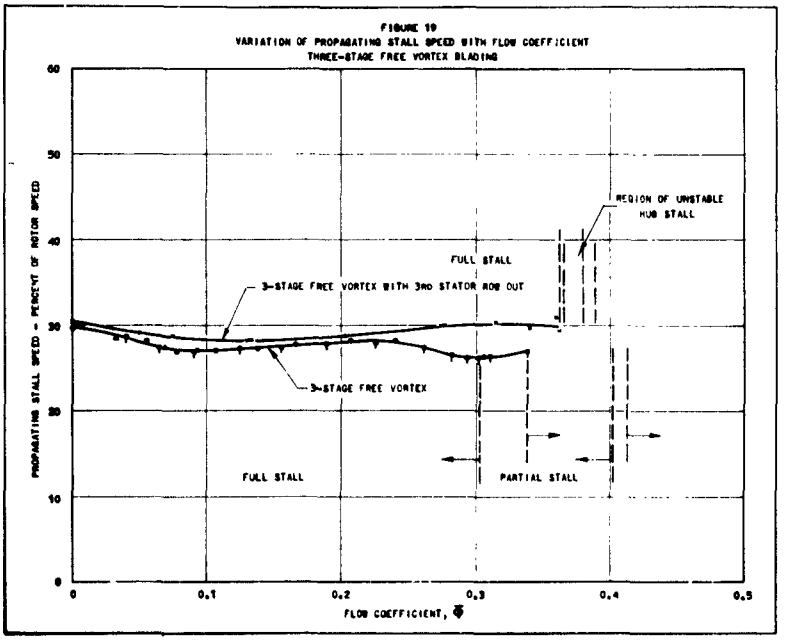

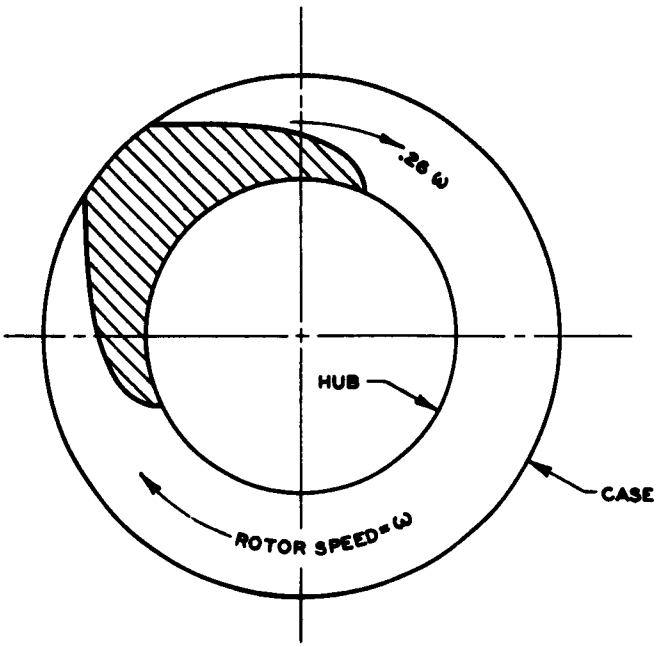

Fig. 20: Depiction of Full Stall Pattern (Looking into Compressor) $\bar{\Phi} = 0.323$ (opening throttle), Three-Stage Free Vortex Blading, Behind Third Rotor Row, 750 rpm

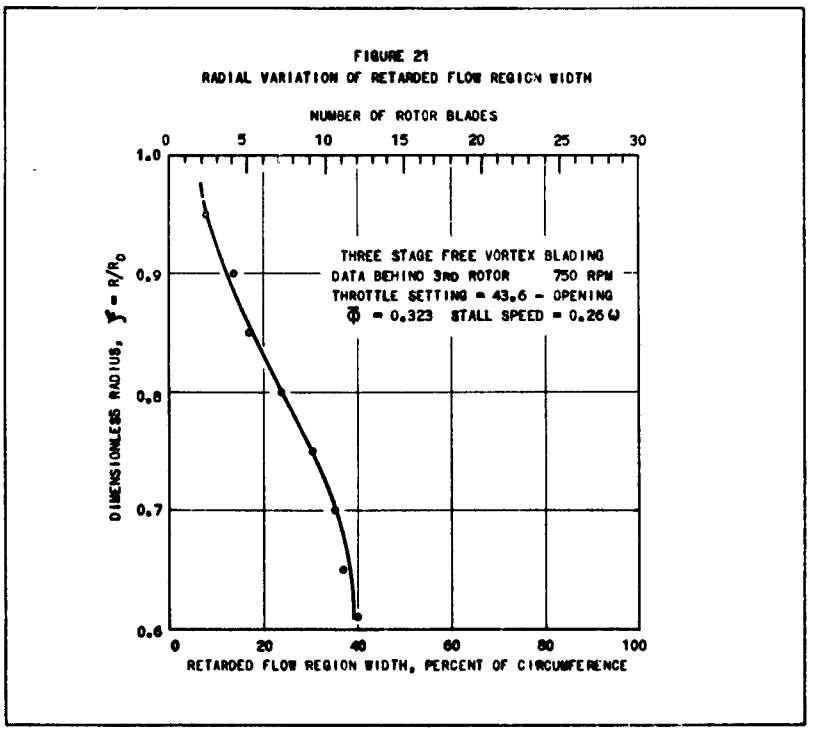

FIGURE 22
VARIATION OF RETARDED FLOW REGION WIDTH WITH FLOW COEFFICIENT
THREE-STAGE FREE VORTEX BLADING
DATA BEHIND THIRD ROTOR AT MID-BLADE HEIGHT, 750 RPM - FULL STALL

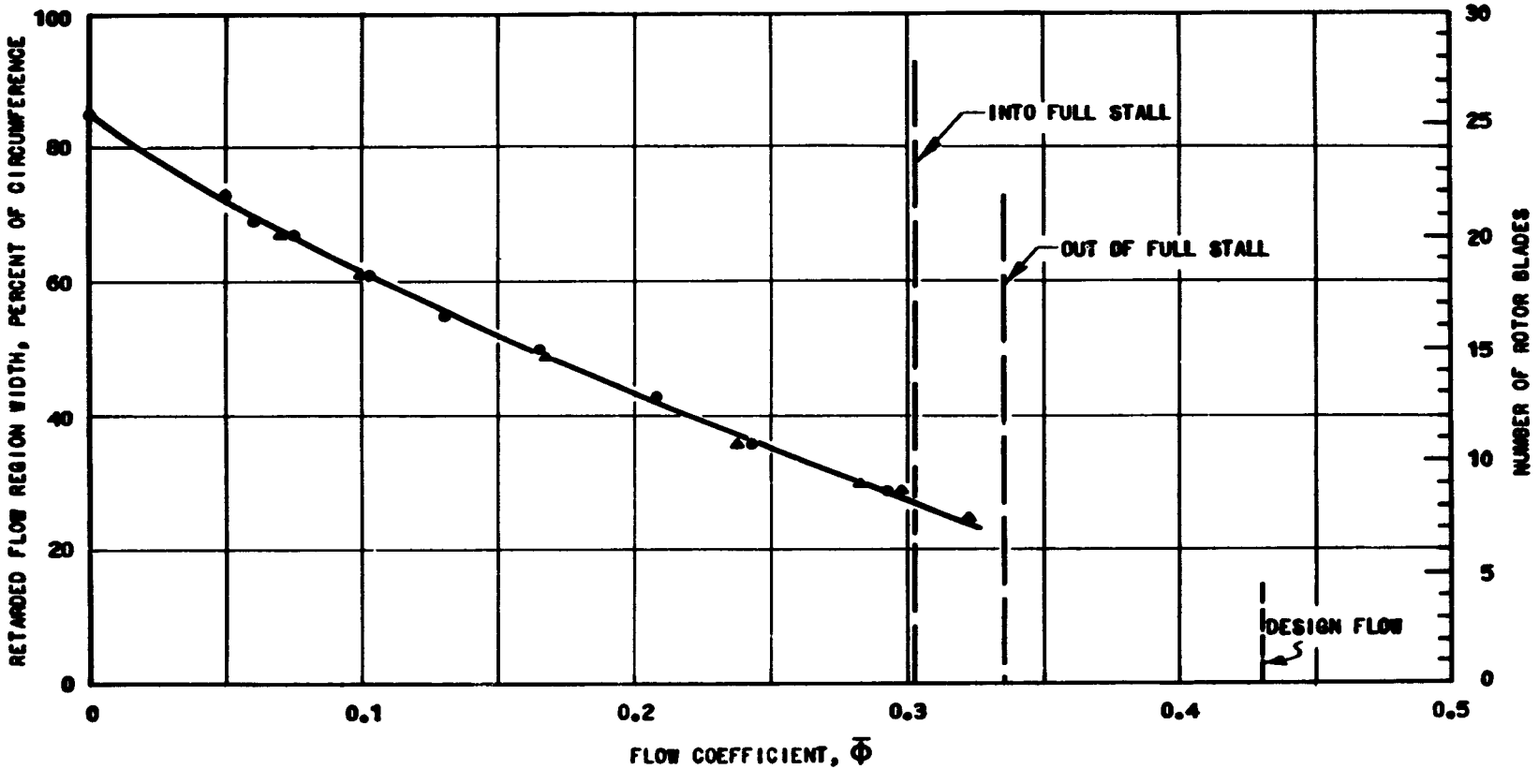

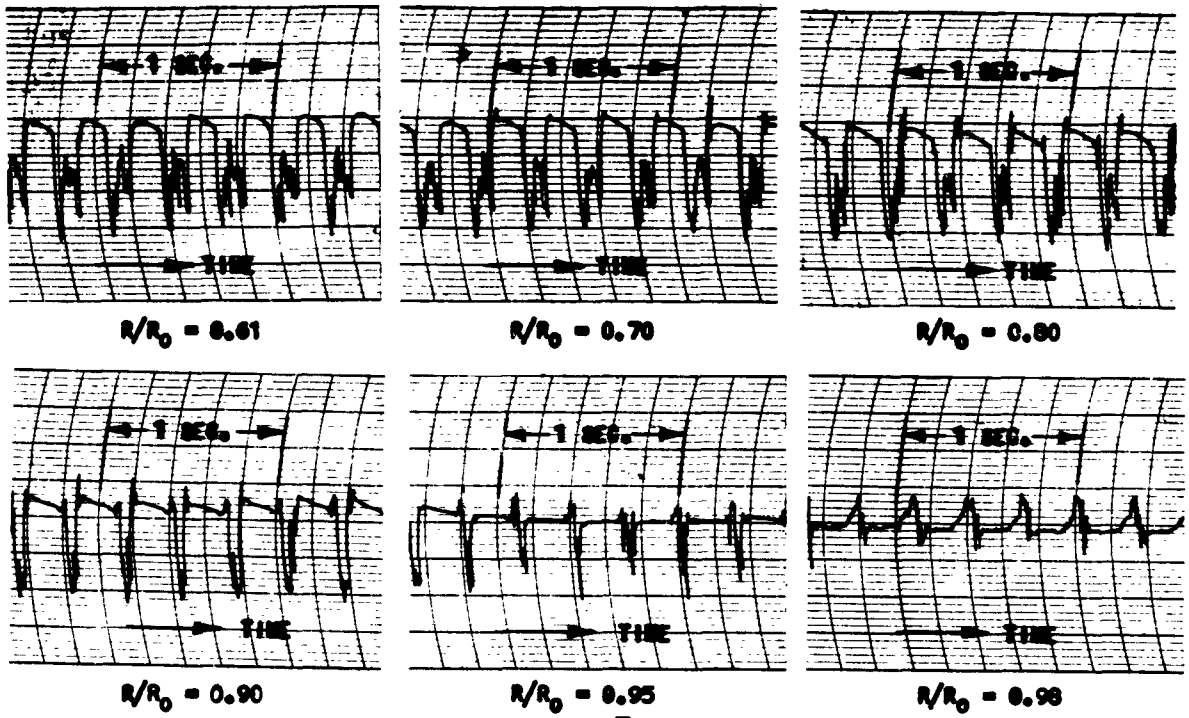

$R/R_0 = 0.61$ $R/R_0 = 0.70$ $R/R_0 = 0.80$

$R/R_0 = 0.90$ $R/R_0 = 0.95$ $R/R_0 = 0.98$

VELOCITY FLUCTUATIONS AT VARIOUS RADII, $\bar{\Phi} = 0.282$, BEHIND THIRD ROTOR ROW.
PROPAGATING STALL SPEED = 26 PERCENT OF ROTOR SPEED.

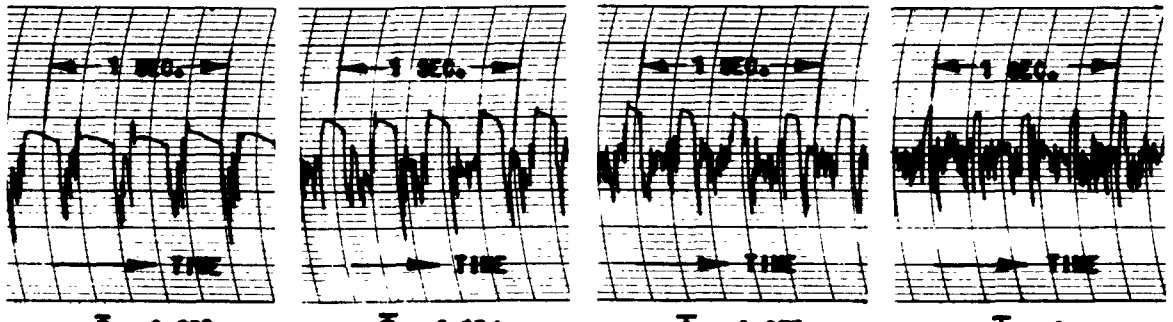

$\bar{\Phi} = 0.293$ $\bar{\Phi} = 0.134$ $\bar{\Phi} = 0.075$ $\bar{\Phi} = 0$

MID-BLADE HEIGHT VELOCITY FLUCTUATIONS AT VARIOUS FLOW COEFFICIENTS
DATA TAKEN BEHIND THIRD ROTOR ROW

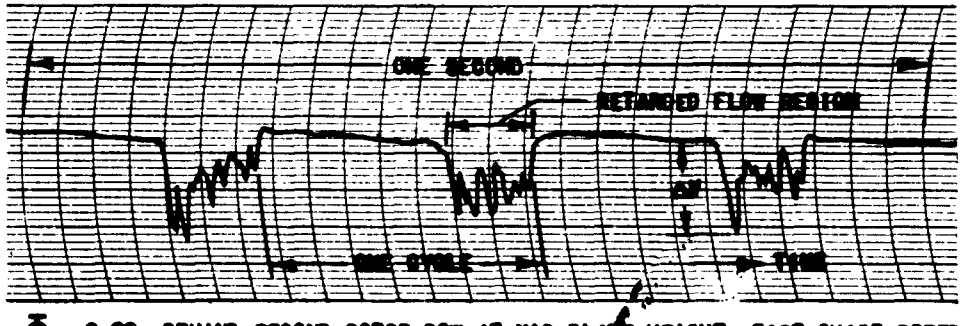

$\bar{\Phi} = 0.29$, BEHIND SECOND ROTOR ROW AT MID-BLADE HEIGHT, FAST CHART SPEED
PROPAGATING STALL SPEED = 26 PERCENT OF ROTOR SPEED

FIGURE 23: OSCILLOGRAPH RECORDS OF FULL STALL VELOCITY FLUCTUATIONS. THREE-STAGE FREE VORTEX BLADING, 750 RPM.

FIGURE 24
THREE STAGE FREE VORTEX BLADING, 750 RPM
DATA TAKEN AT MID-BLADE HEIGHT

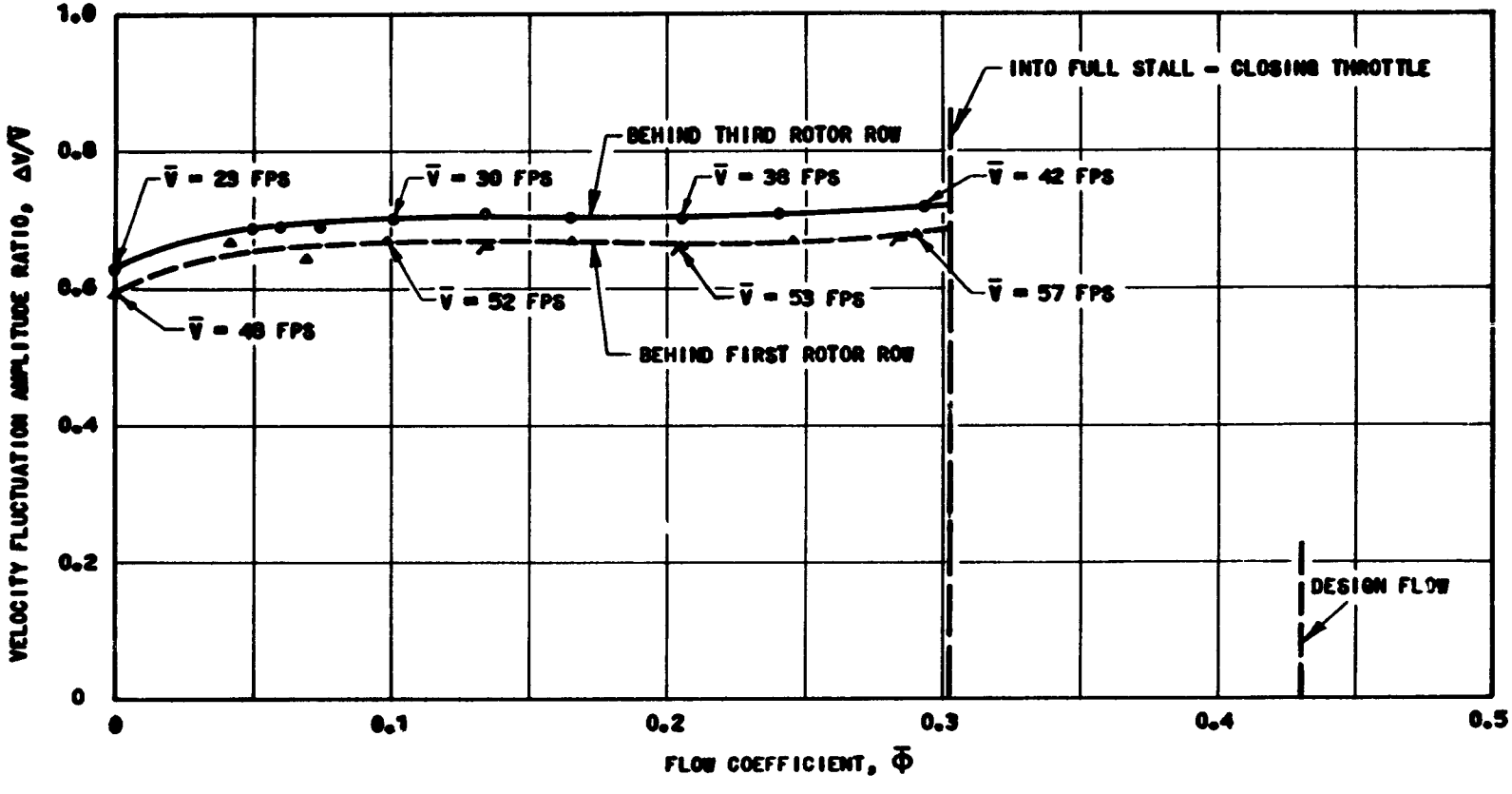

FIGURE 25
VARIATION OF PROPAGATING STALL SPEED WITH FLOW COEFFICIENT
THREE-STAGE FREE VORTEX BLADING, 700 RPM
(ONE-HALF NORMAL COMPLEMENT OF BLADES)
BEHIND THIRD ROTOR

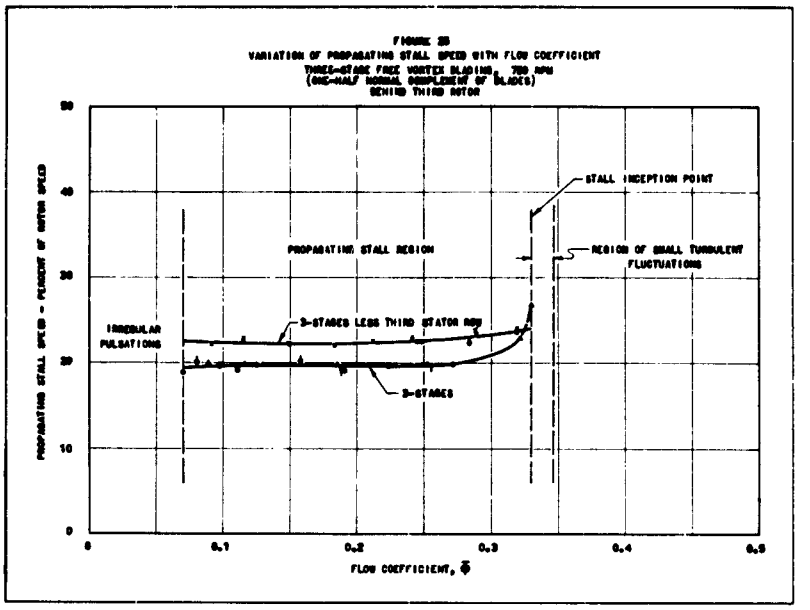

FIGURE 26
EFFECT OF SOLIDITY CHANGE ON PROPAGATING STALL SPEED AT $\bar{\Phi}$ = 0.20
THREE-STAGE FREE VORTEX BLADING

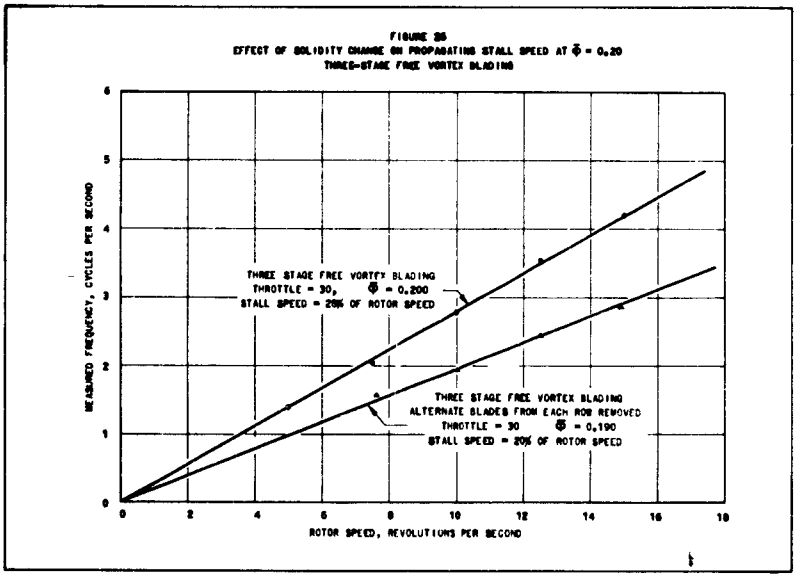

FIGURE 27
VARIATION OF RETARDED FLOW REGION WIDTH WITH FLOW COEFFICIENT
3-STAGE FREE VORTEX BLADING - ALTERNATE BLADES OUT
DATA BEHIND 3RD ROTOR AT $R/R_0 = 0.8$, 750 RPM

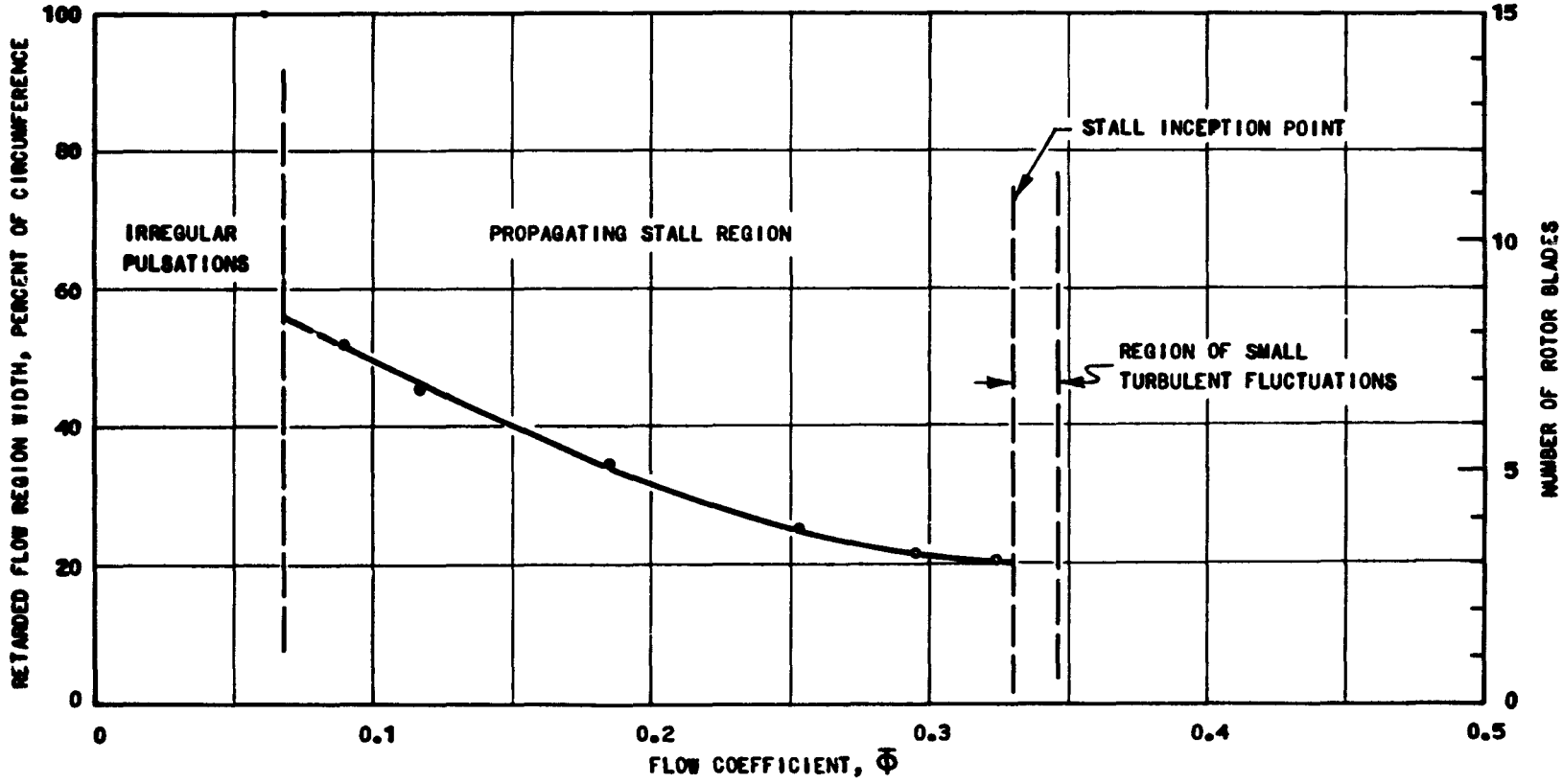

FIGURE 28
RADIAL VARIATION OF RETARDED FLOW REGION WIDTH
THREE-STAGE FREE VORTEX BLADING - 750 RPM
ONE-HALF NORMAL COMPLEMENT OF BLADES
BEHIND THIRD ROTOR

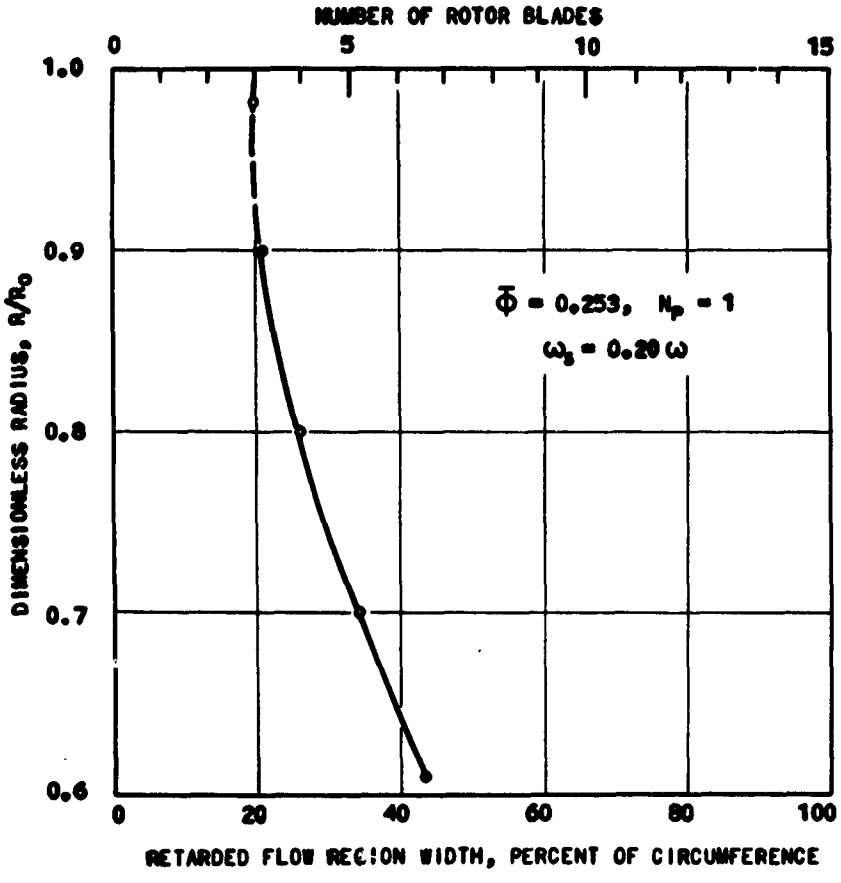

FIGURE 29
VARIATION OF EXIT-DUCT WALL PRESSURE WITH FLOW COEFFICIENT
ONE-STAGE FREE VORTEX BLADING - 720 RPM

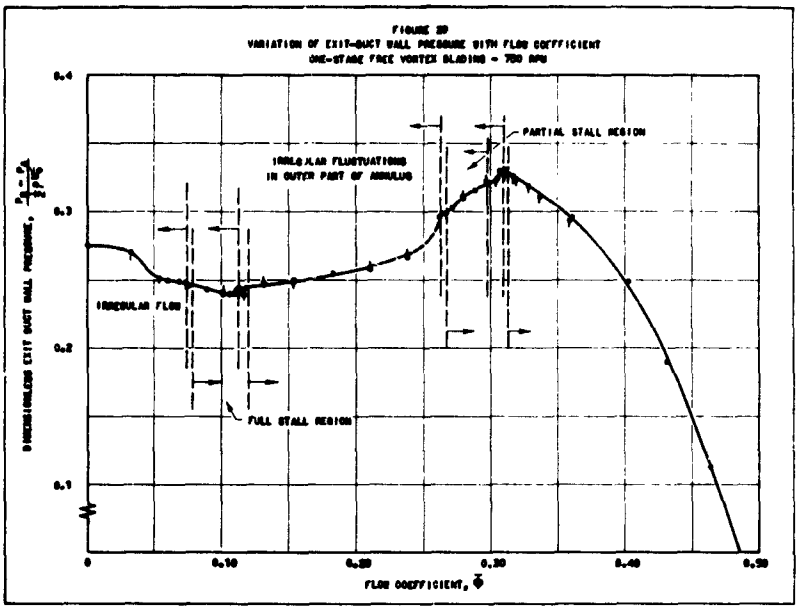

FIGURE 30
VARIATION OF PROPAGATING STALL SPEED WITH FLOW COEFFICIENT
ONE-STAGE FREE VORTEX BLADING - 720 RPM

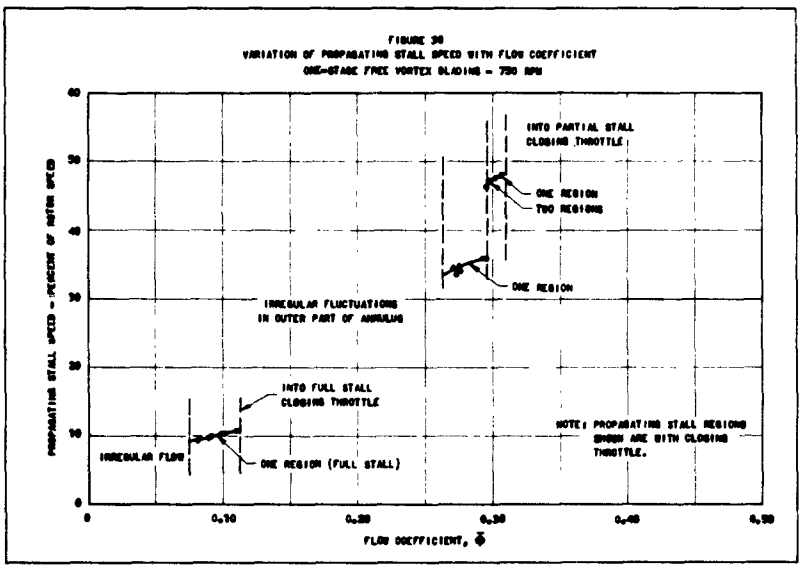

FIGURE 31

RESULTS OF PHASE MEASUREMENTS FOR THE DETERMINATION OF STALL DISTURBANCE NUMBER

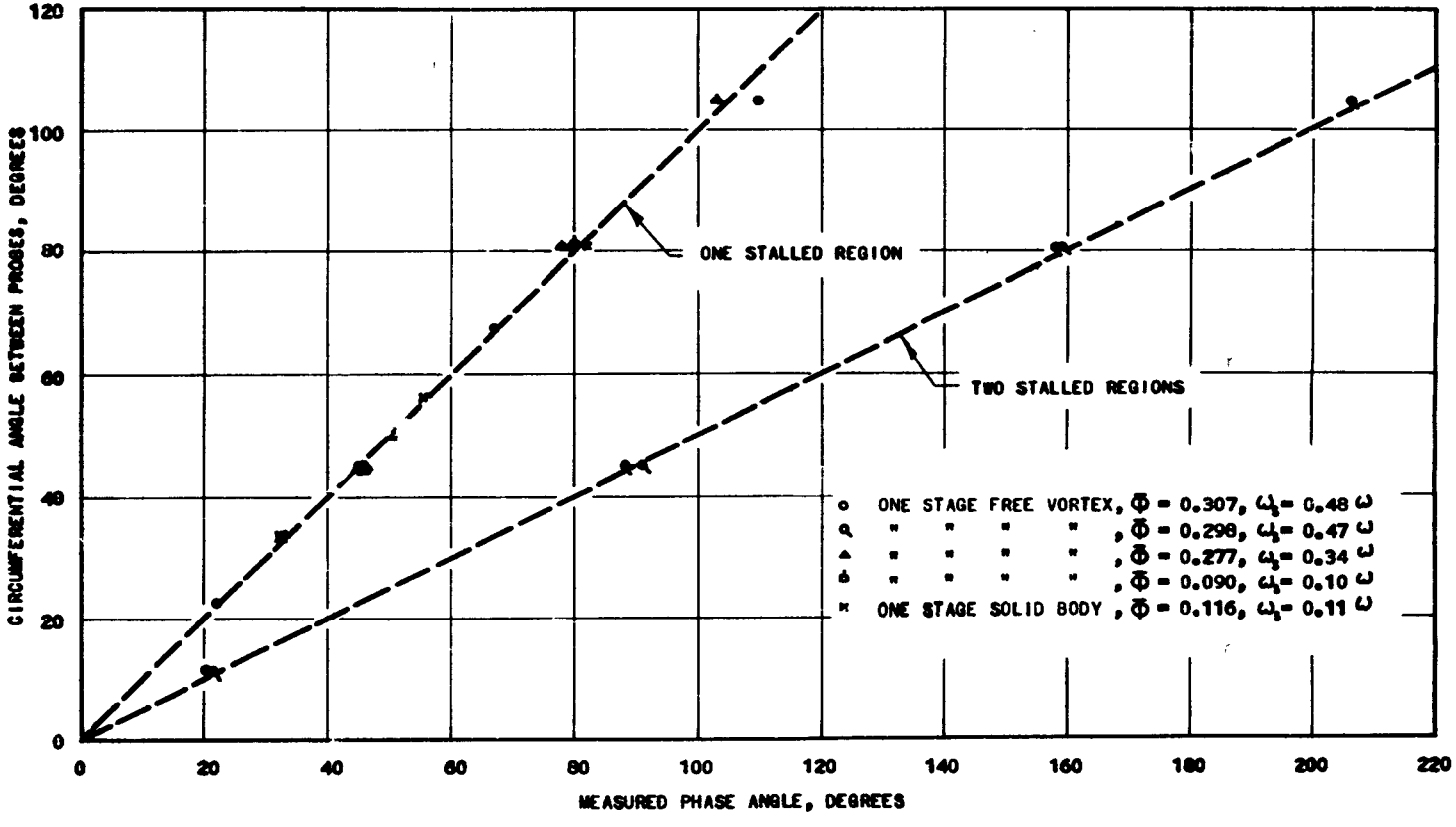

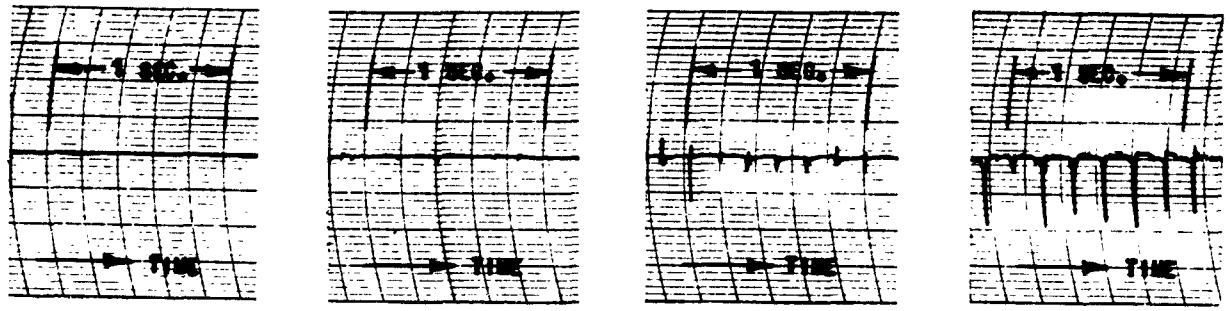

$R/R_0 = 0.70$ $R/R_0 = 0.80$ $R/R_0 = 0.90$ $R/R_0 = 0.98$

ONE-REGION PARTIAL STALL, $\bar{\Phi} = 0.307$ CLOSING THROTTLE, $\omega_s = 0.48\omega$

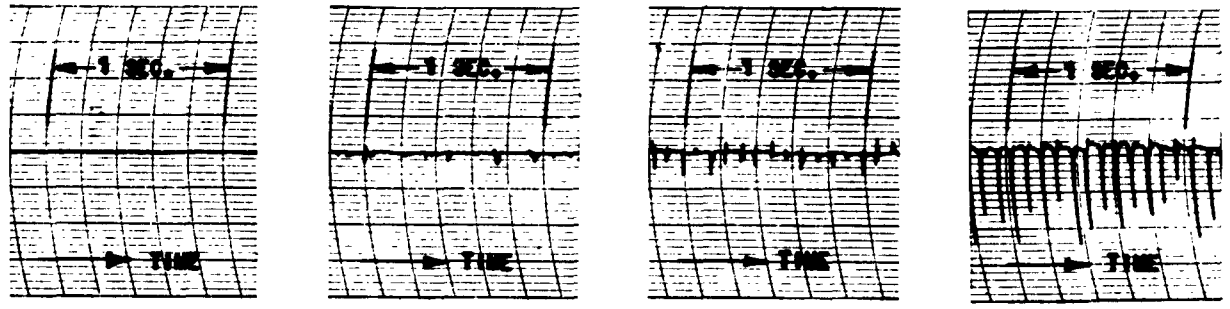

$R/R_0 = 0.65$ $R/R_0 = 0.80$ $R/R_0 = 0.90$ $R/R_0 = 0.98$

TWO-REGION PARTIAL STALL, $\bar{\Phi} = 0.300$ CLOSING THROTTLE, $\omega_s = 0.48\omega$

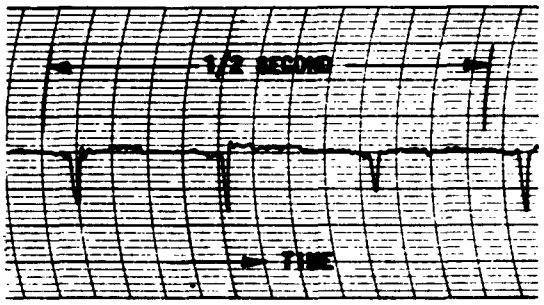

ONE-REGION PARTIAL STALL, $\bar{\Phi} = 0.307$
$R/R_0 = 0.98$, $\omega_s \cong 0.48\omega$, FAST CHART SPEED

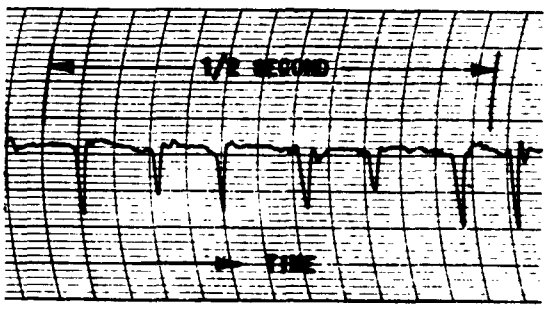

TWO-REGION PARTIAL STALL, $\bar{\Phi} = 0.300$
$R/R_0 = 0.98$, $\omega_s \cong 0.48\omega$, FAST CHART SPEED

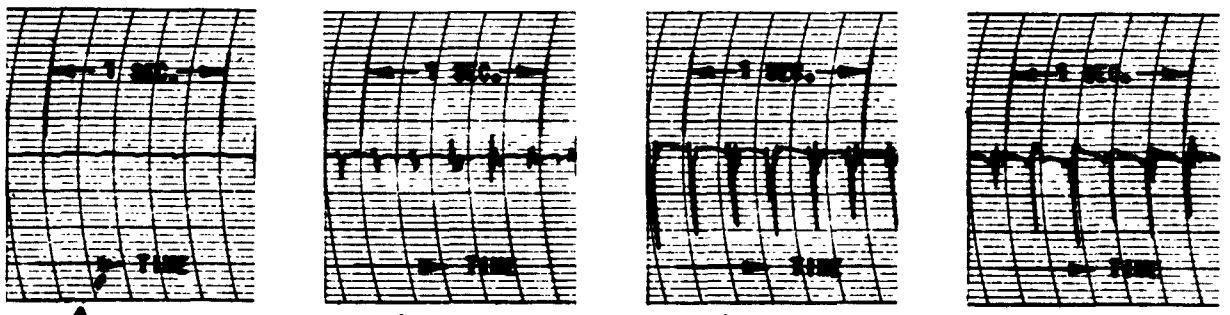

$R/R_0 = 0.61$ $R/R_0 = 0.80$ $R/R_0 = 0.90$ $R/R_0 = 0.98$

ONE-REGION PARTIAL STALL, $\bar{\Phi} = 0.298$ CLOSING THROTTLE, $\omega_s = 0.36\omega$

FIGURE 32: OSCILLOGRAPH RECORDS OF PARTIAL STALL VELOCITY FLUCTUATIONS. DATA BEHIND ROTOR, ONE-STAGE FREE VORTEX BLADING, 750 RPM.

FIGURE 33
RADIAL VARIATION OF VELOCITY FLUCTUATION AMPLITUDE RATIO
ONE STAGE FREE VORTEX BLADING, 720 RPS
BEHIND ROTOR

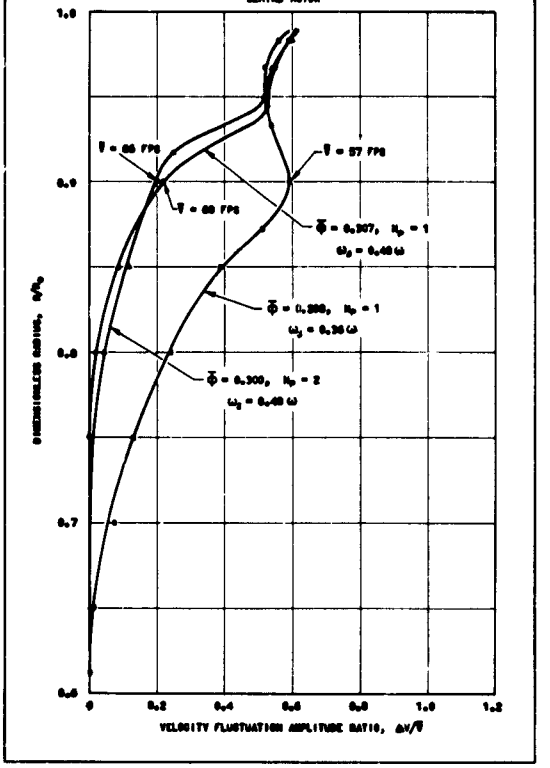

FIGURE 34
RADIAL VARIATION OF VELOCITY FLUCTUATION AMPLITUDE RATIO
ONE STAGE FREE VORTEX BLADING, 720 RPS
BEHIND ROTOR

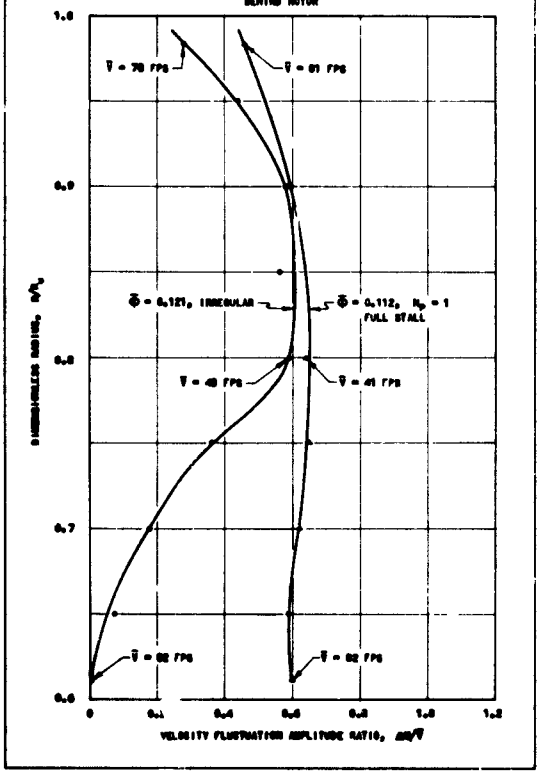

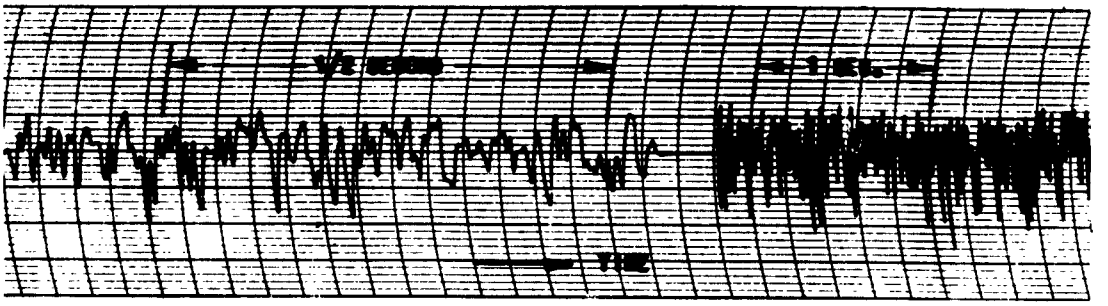

IRREGULAR VELOCITY FLUCTUATIONS IN OUTER PART OF ANNULUS. $\bar{\phi} = 0.160$ CLOSING THROTTLE
$R/R_0 = 0.950$, CHART SPEEDS OF 125 MM/SEC. AND 25 MM/SEC.

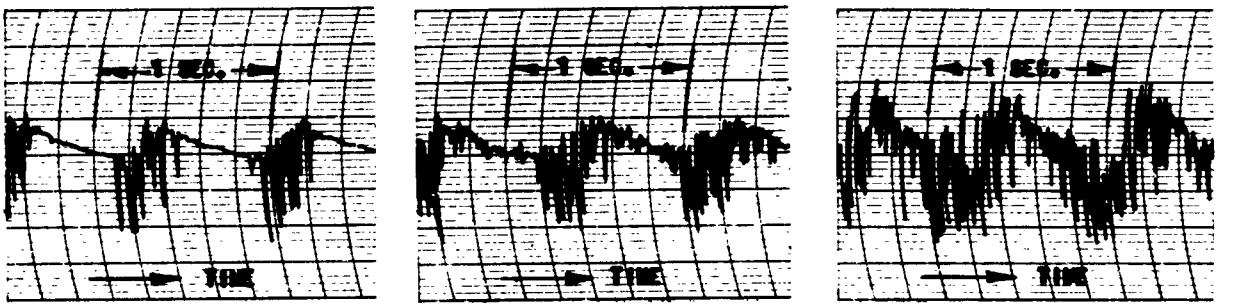

$R/R_0 = 0.61$ $R/R_0 = 0.70$ $R/R_0 = 0.80$

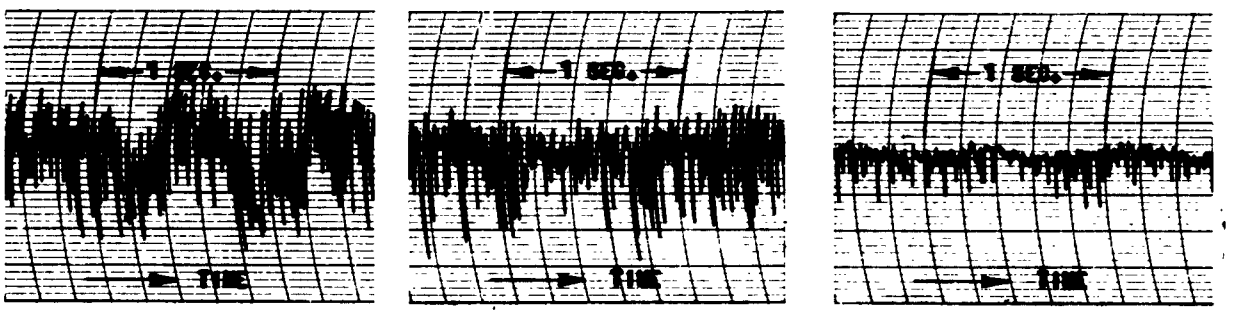

$R/R_0 = 0.90$ $R/R_0 = 0.95$ $R/R_0 = 0.98$

FULL STALL VELOCITY FLUCTUATIONS AT VARIOUS RADII. $\bar{\phi} = 0.090$ CLOSING THROTTLE
PROPAGATING STALL SPEED = 10 PERCENT OF ROTOR SPEED

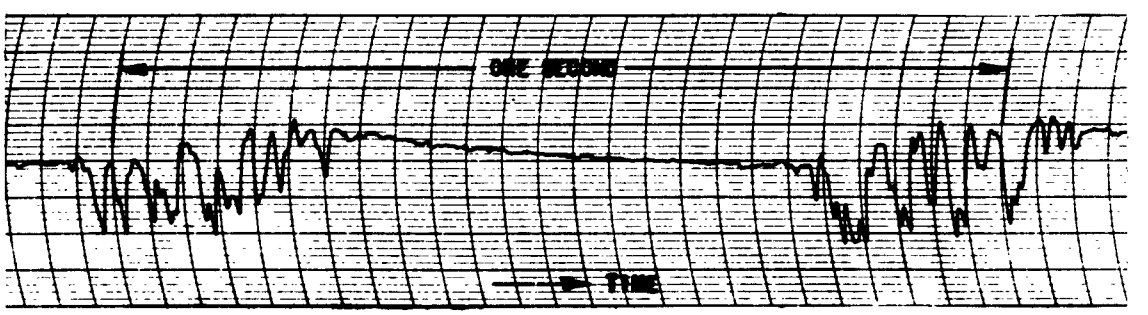

FULL STALL VELOCITY FLUCTUATIONS $\bar{\phi} = 0.090$, $R/R_0 = 0.61$, $\omega_s = 0.10\omega$
FAST CHART SPEED (125 MM/SEC.)

FIGURE 35: OSCILLOGRAPH RECORDS OF VELOCITY FLUCTUATIONS. ONE-STAGE FREE VORTEX BLADING DATA BEHIND ROTOR ROW, 750 RPM.

FIGURE 36
RADIAL VARIATION OF RETARDED FLOW REGION WIDTH

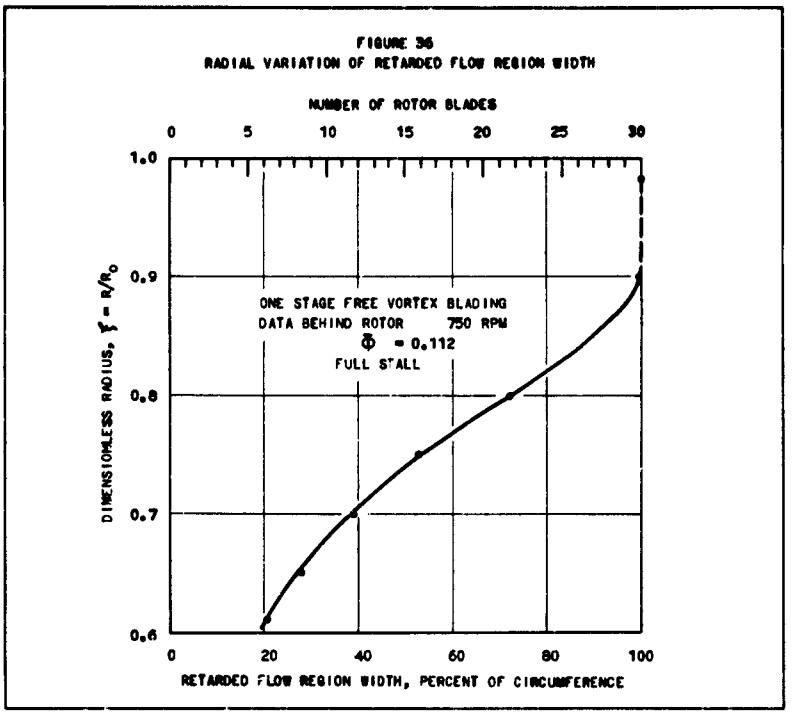

FIGURE 37
VARIATION OF RETARDED FLOW REGION WIDTH WITH FLOW COEFFICIENT
ONE-STAGE FREE VORTEX BLADING - 750 RPM
BEHIND ROTOR AT $R/R_o = 0.611$

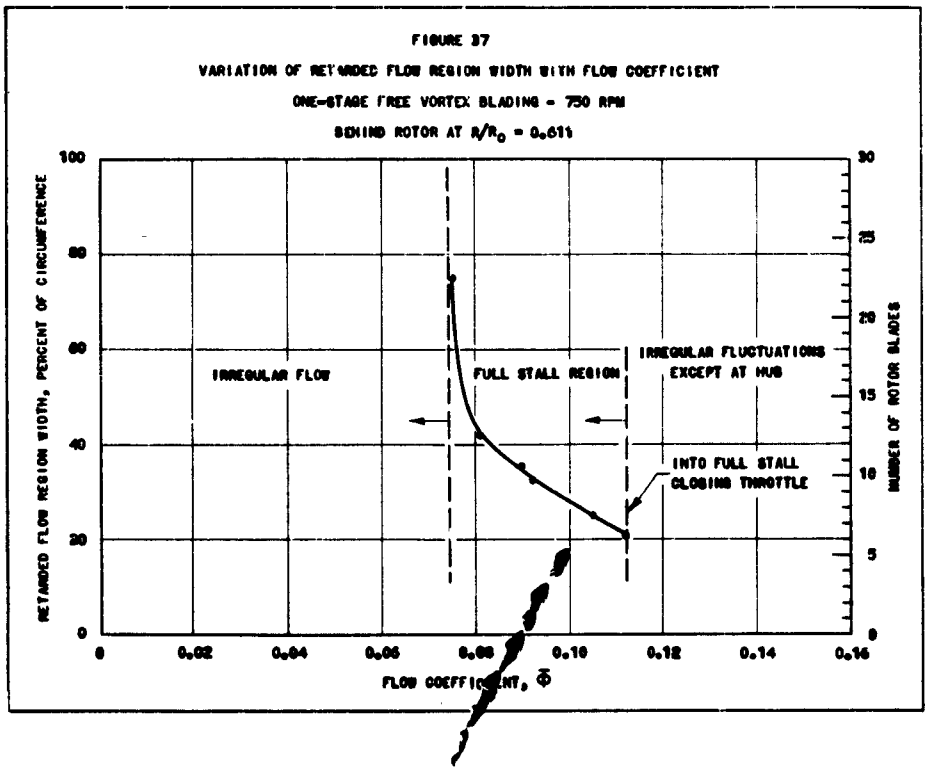

FIGURE 38
VARIATION OF EXIT-DUCT WALL PRESSURE WITH FLOW COEFFICIENT
ONE-STAGE SOLID BODY BLADING - 750 RPM

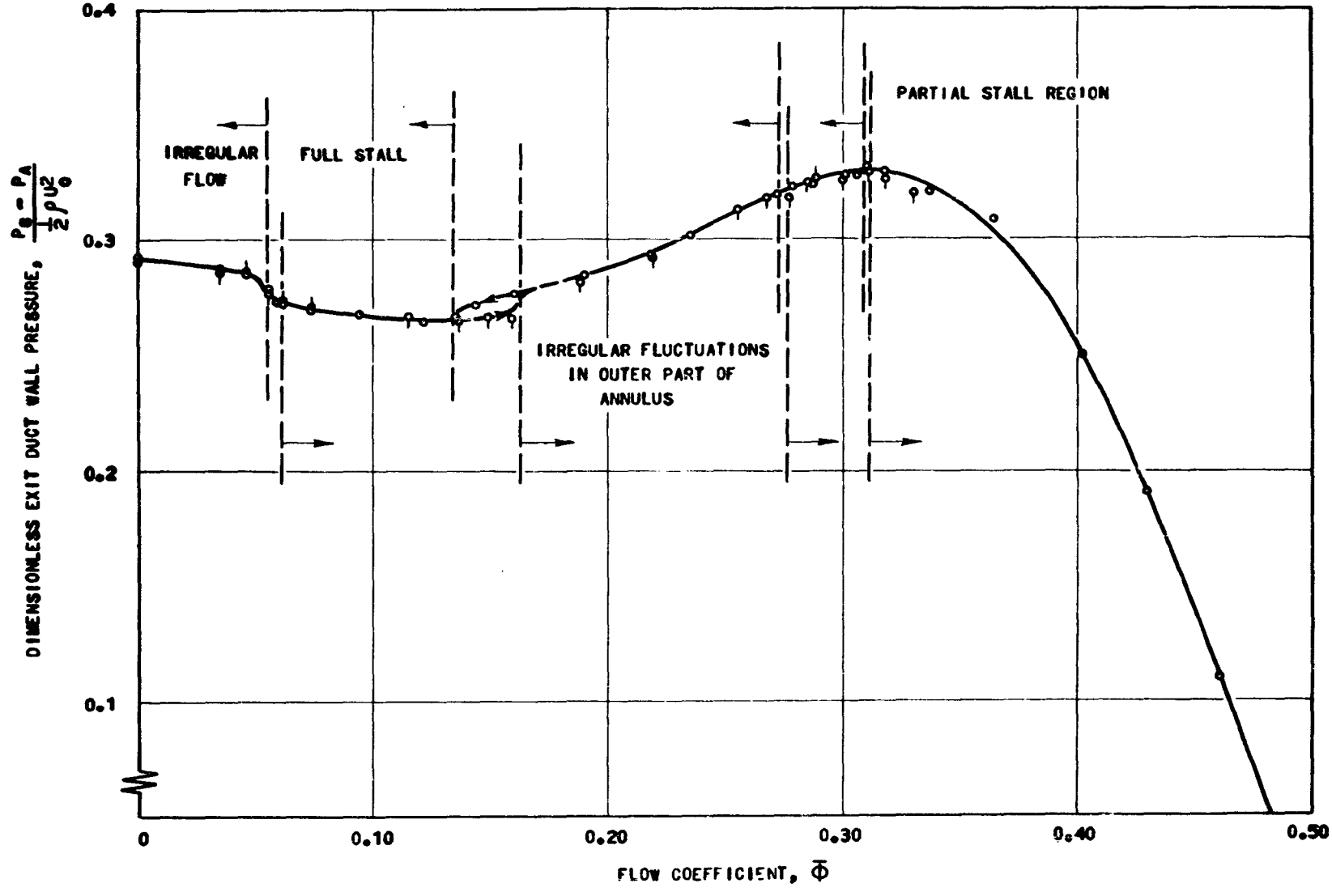

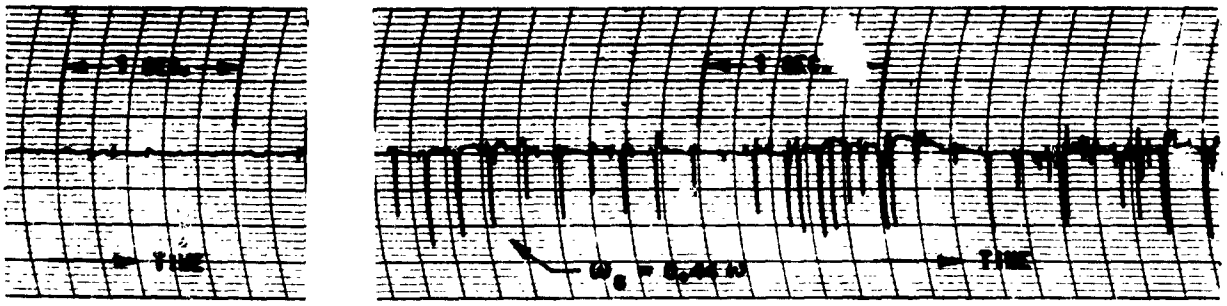

$R/R_0 = 0.80$ $R/R_0 = 0.983$

ONE-REGION PARTIAL STALL (UNSTABLE), $\bar{\Phi} = 0.308$ CLOSING THROTTLE, INITIAL STALL POINT.

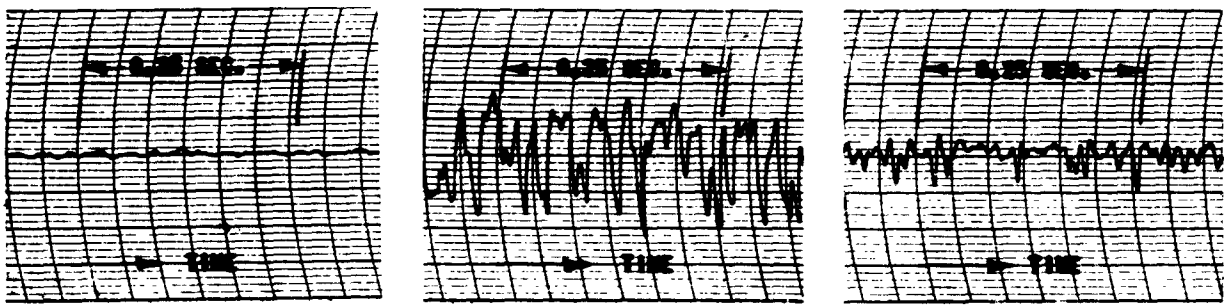

$R/R_0 = 0.611$ $R/R_0 = 0.800$ $R/R_0 = 0.983$

IRREGULAR VELOCITY FLUCTUATIONS, LARGELY IN OUTER PART OF ANNULUS, $\bar{\Phi} = 0.139$ CLOSING THROTTLE
FAST CHART SPEED (125 MM/SEC.)

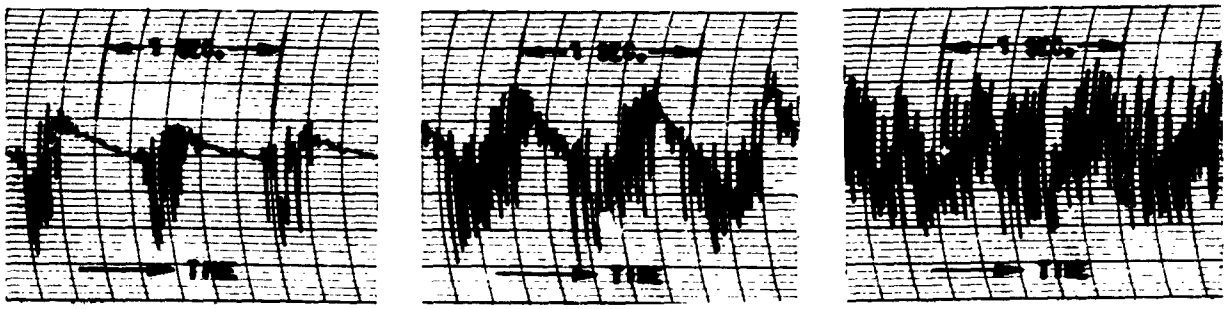

$R/R_0 = 0.700$ $R/R_0 = 0.800$ $R/R_0 = 0.900$

FULL STALL VELOCITY FLUCTUATIONS AT VARIOUS RADII. $\bar{\Phi} = 0.129$ CLOSING THROTTLE, $\omega_s = 0.11\omega$
(INTERMEDIATE CHART SPEED - 25 MM/SEC.)

FIGURE 39: OSCILLOGRAPH RECORDS OF VELOCITY FLUCTUATIONS.
ONE-STAGE SOLID BODY BLADING, BEHIND ROTOR,
750 RPM.

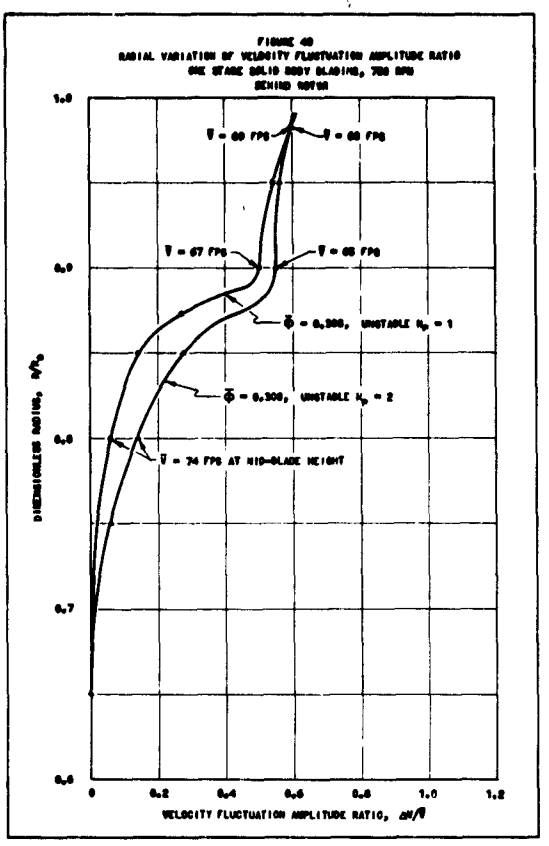

FIGURE 40
RADIAL VARIATION OF VELOCITY FLUCTUATION AMPLITUDE RATIO
ONE STAGE SOLID BODY BLADING, 700 RPS
BEHIND ROTOR

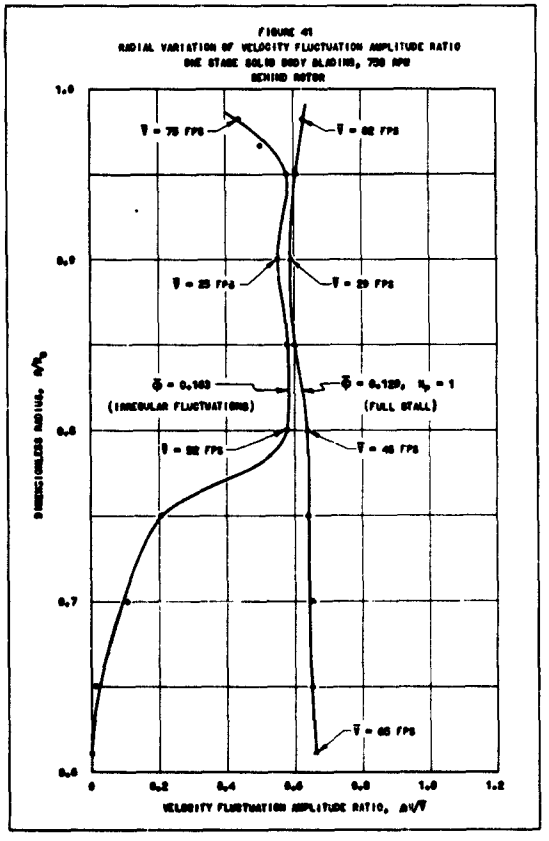

FIGURE 41
RADIAL VARIATION OF VELOCITY FLUCTUATION AMPLITUDE RATIO
ONE STAGE SOLID BODY BLADING, 700 RPS
BEHIND ROTOR

FIGURE 42
VARIATION OF FULL STALL PROPAGATING STALL SPEED WITH FLOW COEFFICIENT
ONE-STAGE SOLID BODY BLADING - 750 RPM
DATA BEHIND ROTOR

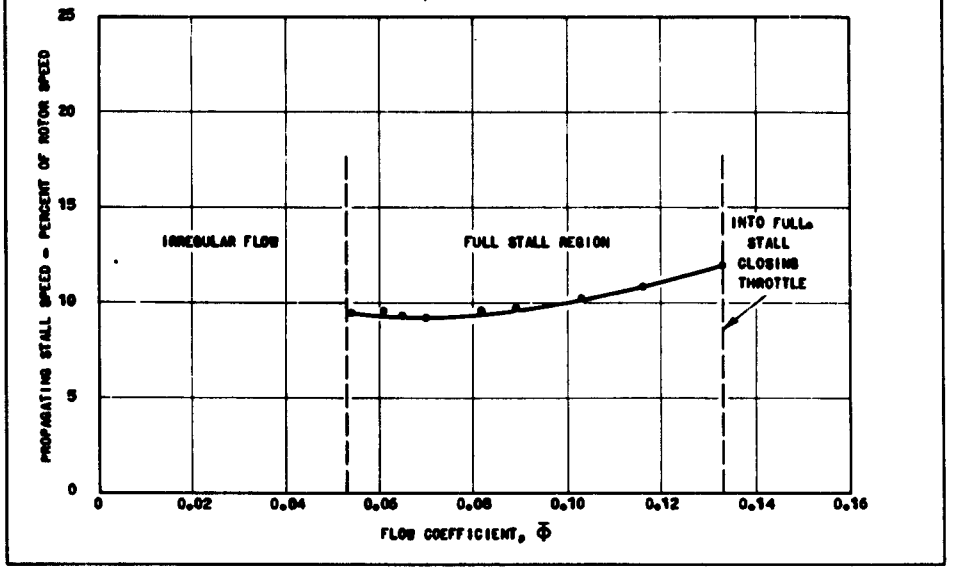

FIGURE 43
VARIATION OF RETARDED FLOW REGION WIDTH WITH FLOW COEFFICIENT
ONE-STAGE SOLID BODY BLADING - 750 RPM
BEHIND ROTOR AT $R/R_0 = 0.611$

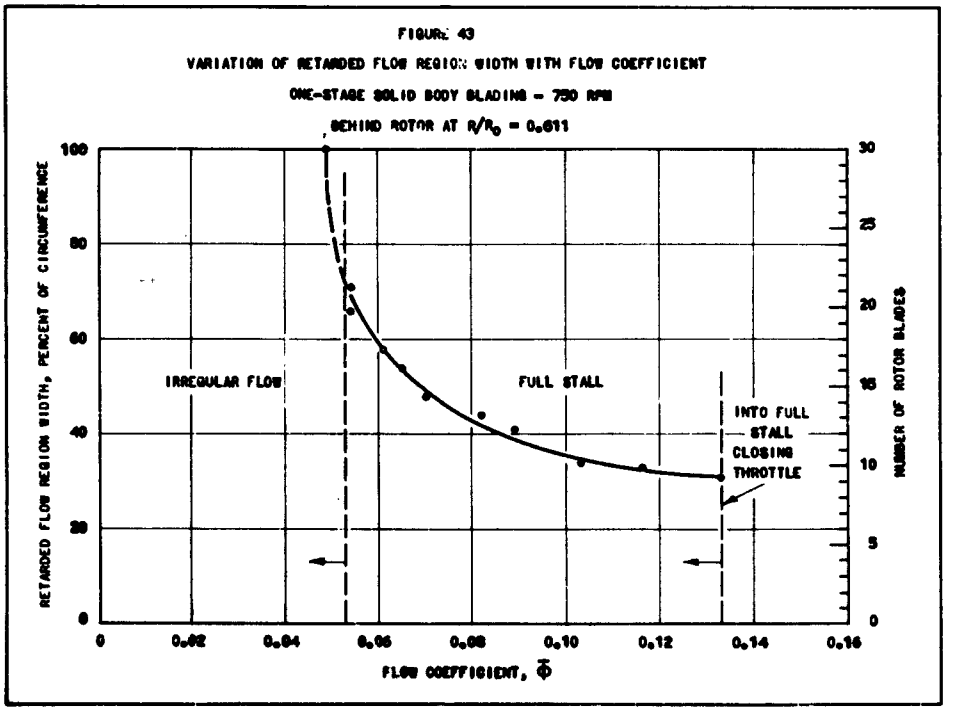

FIGURE 44
RADIAL VARIATION OF RETARDED FLOW REGION WIDTH